Joint Optimization for Traffic-Offloading and Resource-Allocation Over RF-Powered Backscatter Mobile Wireless Networks

Fei Wang and Xi Zhang, *Fellow, IEEE*

***Abstract*—We develop the joint optimization schemes for traffic-offloading and resource-allocation over radio-frequency (RF) powered backscatter-based mobile wireless networks, where a macro-cell base station (BS), several small-cell access points (SAPs), and multiple energy harvesting (EH) mobile users (MUs) co-exist. Optimizing MUs' network access (via traffic-offloading) and system resource-allocation, we aim to minimize MUs' energy consumption by using low-energy consumption of backscatter. First, we consider the scenarios when short-range ambient backscatter (AB) communication (e.g., over several meters) is employed, enabling MUs to access nearby SAPs via ambient backscatter RF signals for data transmission. Using the alternating directions method of multipliers (ADMM), we develop a distributed traffic-offloading and resource-allocation scheme. Then, we focus on traffic-offloading and resource-allocation by adopting the concurrent AB (CAB) transmission, where multiple MUs can backscatter data concurrently to further reduce energy consumption. Moreover, we also use long-range bi-static backscatter (BB) communication (e.g., over 270-meter distance) for data transmission between MUs and BS, and then MUs can convey data by backscattering RF signals radiated from dedicated carrier emitters. Then, we study the joint traffic-offloading and resource-allocation when AB and BB communications are adopted by MUs accessing SAPs and BS, respectively. Finally, the numerical analyses validate and evaluate our developed schemes, showing their good convergence performances and significant reduction in energy consumption of MUs through backscatter communications.**

***Index Terms*—RF energy harvesting, ambient and bistatic backscatters, traffic-offloading, resource-allocation, ADMM.**

I. Introduction

RECENTLY, radio-frequency (RF) based energy harvesting (EH) has attracted significant attention for wireless networks, through which mobile users (MUs) can transmit data using the energy harvested from RF signals radiated by ambient or dedicated energy sources. However, system performance may not be guaranteed when MUs cannot harvest sufficient energy [1]. One particularly promising solution to improve system performance of RF-powered wireless networks is to utilize the backscatter communications. Without any form of active radio transmission, the backscatter communications enable MUs to convey information by backscattering incident RF signals via tuning the antenna impedance [2], [3]. Hence, the energy consumption of the backscatter communications is very low (typically a few μW) [1]. There are two popular types of backscatter communications, i.e., the ambient backscatter (AB) [3]–[5] and the bistatic backscatter (BB) [6], which rely on different incident RF signal sources.

The AB communication, which was first proposed in [3], uses ambient RF signals, e.g., TV signals, as incident RF signals [5]. The hardware prototype built in [3] can support a backscatter rate of up to 10 kbps at a range of about 0.5 meter by averaging out the ambient TV signals. The authors of [4] designed a multi-antenna backscatter receiver, i.e., μmo, and a low-power coding mechanism, i.e., μcode, to improve the backscatter rate (up to 1 Mbps) and the communication range (up to about 24 meters but with low backscatter rate, i.e., 1 kbps) of the AB communication, respectively. The authors of [7] developed a novel AB communication system, i.e., BackFi, which can achieve a backscatter rate of 1 Mbps at a range of 5 meters and a backscatter rate of 5 Mbps at a range of 1 meter. However, due to the limited communication range, the AB communication may only be suitable for short-range communications [8]. The BB communication, which was first proposed in [6], utilizes unmodulated carrier signals radiated from dedicated carrier emitters (CEs) as incident RF signals [8]. The BB architecture designed in [6] can achieve a backscatter rate of 1 Kbps at a range of 130 meters. The BB prototypes developed in [9], [10] extended the communication range to 250 meters and about 270 meters, respectively. Therefore, the BB communication can support a long communication range compared with the AB communication.

In [1], the authors first introduced the short-range AB communication into RF-powered cognitive radio networks, where secondary users (SUs) can either backscatter primary signals for data transfer, i.e., working in the AB mode, or transmit data using the previously harvested energy, i.e., working in the harvest-then-transmit (HTT) mode. The authors of [1], [11], [12] studied the tradeoff between the HTT mode and the AB

Manuscript received January 17, 2021; revised May 26, 2021 and June 24, 2021; accepted June 25, 2021. Date of publication August 10, 2021; date of current version October 4, 2021. The work of Fei Wang was supported by Zhejiang Lab under Grant 2021LC0AB01. The work of Xi Zhang was supported in part by the U.S. National Science Foundation under Grants: CCF-2142890, CCF-2008975, ECCS-1408601, and CNS-1205726. The guest editor coordinating the review of this manuscript and approving it for publication was Prof. Mohamed Alouini. *(Corresponding author: Xi Zhang.)*

Fei Wang is with the College of Electronic and Information Engineering, Southwest University, Chongqing 400715, China (e-mail: wsf0107@163.com).

Xi Zhang is with the Networking and Information Systems Laboratory, Department of Electrical and Computer Engineering, Texas A&M University, College Station, TX 77843 USA (e-mail: xizhang@ece.tamu.edu).

Digital Object Identifier 10.1109/JSTSP.2021.3102391

1932-4553 © 2021 IEEE. Personal use is permitted, but republication/redistribution requires IEEE permission.
See https://www.ieee.org/publications/rights/index.html for more information.

Authorized licensed use limited to: Texas A M University. Downloaded on January 17,2022 at 20:42:04 UTC from IEEE Xplore. Restrictions apply.

mode for EH-based MUs in RF-powered wireless networks. Moreover, the authors of [13], [14] considered the time scheduling problem for RF-powered backscatter IoT networks, where the time scheduling of multiple communication modules, e.g., the AB mode, is studied for IoT devices. The authors of [15], [16] studied the resource-allocation problem for RF-powered wireless networks using the long-range BB communication, where MUs convey data by backscattering RF signals emitted from dedicated CEs deployed nearby. In [8] and [17], integrating the AB communication and the BB communication, the authors considered the hybrid backscatter communications for RF-powered IoT networks to increase the communication range of IoT devices. However, all the above works, i.e., [1], [8], and [11]–[17], only consider the resource-allocation and/or the time scheduling for RF-powered backscatter wireless networks when the serving base station (BS) or access point (AP) (e.g., small-cell or WiFi) is given for each MU or IoT device. The problem of joint traffic-offloading and resource-allocation has hardly been studied for RF-powered backscatter wireless networks, where through traffic-offloading MUs or IoT devices using backscatter can dynamically access suitable BSs or APs for data transmission [18] to minimize the EH-based MUs' or IoT devices' energy consumption and/or delay, which are two important quality-of-service (QoS) metrics [19]–[25]. Hence, with the rapid increase of mobile data traffic, how to design suitable traffic-offloading and resource-allocation schemes for RF-powered backscatter wireless networks deserves much timely research attention and efforts.

To overcome the above challenges, in this paper we propose to develop the joint traffic-offloading and resource-allocation schemes for RF-powered backscatter-based mobile wireless networks, where a macro-cell BS, several small-cell APs (SAPs), e.g., femtocell APs, and multiple EH-based MUs coexist. We aim to minimize the overall energy consumption of MUs by jointly optimizing MUs' network access (through traffic-offloading) and system resource-allocation. Our main contributions can be summarized as follows:

- First, we propose the joint optimization for traffic-offloading and resource-allocation over RF-powered mobile wireless networks by using the short-range AB communication, where MUs can dynamically access the BS or one SAP for data transmission. Leveraging the alternating directions method of multipliers (ADMM), we decompose the formulated optimization problem into several subproblems, and propose a distributed traffic-offloading and resource-allocation scheme, based on which MUs accessing nearby SAPs can dynamically work in the AB mode or the HTT mode to reduce energy consumption.
- Then, adopting the novel coding mechanism μcode [4], which enables the concurrent AB communication of multiple MUs, we propose the joint traffic-offloading and resource-allocation scheme when MUs can work in the concurrent AB (CAB) mode [4]. Based on the solution to the scenario which considers the AB mode, we develop a clustering algorithm to group MUs into different clusters, and allow MUs in the same cluster to backscatter data concurrently for efficient utilization of the CAB mode.

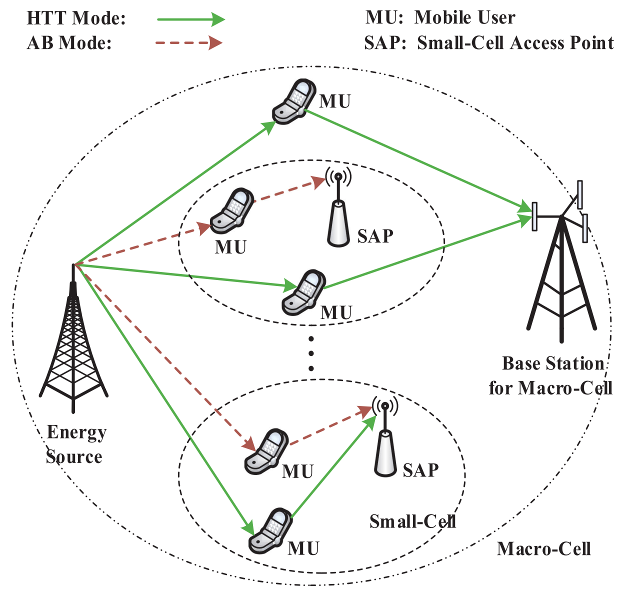

Fig. 1. The system architecture model for our proposed RF-powered mobile networks, where an MU can switch between the harvest-then-transmit (HTT) mode and the ambient backscatter (AB) mode when accessing the SAPs for traffic-offloading. If an MU is not accessible to any small cell's SAP, it transmits data to the macro-cell base station using the HTT mode.

- Furthermore, to reduce the energy consumption of MUs accessing the BS, we leverage the long-range BB communication to support the data transmission between MUs and the BS. Accordingly, we solve the joint traffic-offloading and resource-allocation optimization problem, and propose the corresponding traffic-offloading and resource-allocation scheme for the scenario when the AB and BB communications can be utilized by MUs accessing the SAP and the BS, respectively.
- Finally, we conduct extensive numerical analyses to validate and evaluate the performance of our proposed traffic-offloading and resource-allocation schemes. The numerical results show that our proposed schemes have competitive convergence performance and can significantly reduce the energy consumption of MUs. Moreover, the energy consumption of MUs obtained by our schemes is very close to that obtained by the centralized algorithm.

The rest of this paper is organized as follows. Section II establishes the system model. Sections III-IV develop the joint traffic-offloading and resource-allocation schemes. Section V conducts the numerical analyses and evaluations. The paper concludes with Section VI.

II. The System Architecture Models

A. Network Architecture

Figure 1 shows the system architecture model for our proposed radio-frequency (RF) powered mobile wireless networks, which consists of a macro-cell base station (BS) b_0, N small-cell access points (SAPs), e.g., femtocell APs, and K energy harvesting (EH) based mobile users (MUs). All MUs are low-power

Authorized licensed use limited to: Texas A M University. Downloaded on January 17,2022 at 20:42:04 UTC from IEEE Xplore. Restrictions apply.

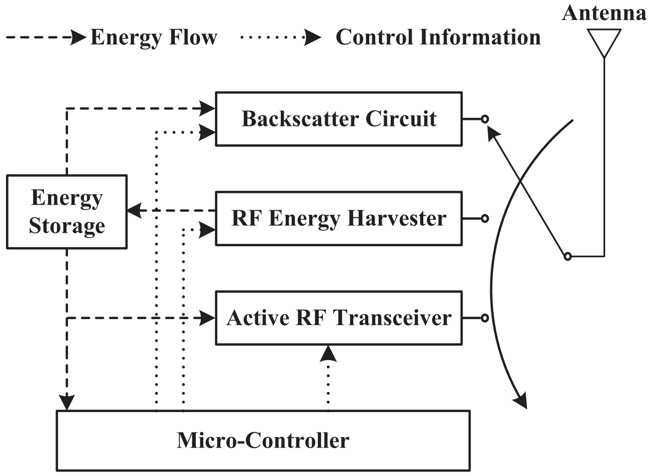

Fig. 2. System architecture model for the RF-powered backscatter MUs.

devices, e.g., wireless sensors, and they are powered by an ambient energy source (ES). Each MU k, $k \in \mathcal{K} \triangleq \{1, \ldots, K\}$, is covered not only by the BS b_0 but also by several SAPs in $\mathcal{N} \triangleq \{1, \ldots, N\}$. For relieving the traffic burden of the BS b_0, MU k can select one nearby SAP n, $n \in \mathcal{N}$, for data transmission, which is called the traffic-offloading [18].

Similar to [1], [12], each MU k is composed of five main components as shown in Fig. 2, i.e., a micro-controller, an active RF transceiver, a backscatter circuit,[1] an RF energy harvester, and an energy storage, e.g., a capacitor. Therefore, MU k can work in the harvest-then-transmit (HTT) mode, where it first harvests energy from the ES's RF signals using the RF energy harvester and stores the harvested energy in the energy storage, and then through active radio transmission, it leverages the harvested energy for data transmission using the active RF transceiver. Furthermore, MU k can also work in the ambient backscatter (AB) mode, where instead of generating radio waves as in the active radio transmission, MU k performs passive communication by modulating its own information bits to the ES's RF signals and backscattering the ES's signals to convey information using the backscatter circuit [17]. Hence, for MU k, the power consumption in the AB mode (typically a few μW) is much lower than that in the HTT mode. The achievable rate and the communication range of the AB technique depend on the specific design of the backscatter transceiver [8]. Generally, the communication range of the AB technique is several meters, with up to about 24 meters but with very low backscatter rate, i.e., 1 kbps [4]. Therefore, we assume that MU k can switch between the HTT mode and the AB mode adaptively when accessing nearby SAPs [1].[2] However, MU k can only work in the HTT mode when accessing the BS b_0, which generally will not be deployed too close to MUs. The micro-controller is responsible for controlling the overall operation of MU k, e.g., the switch between the AB and the HTT modes.

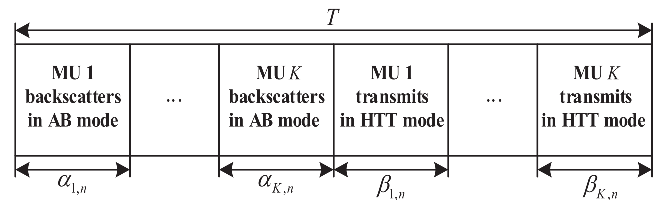

Fig. 3. The cooperation between MUs and SAP n, $\forall n \in \mathcal{N}$, aided by the AB communication.

The considered system is time-slotted, with the duration of each time slot being T. When MU k accesses the BS b_0, it works in the HTT mode, where the energy harvesting and data transmission occur in two phases. In the first phase with duration $\vartheta_{k,\mathrm{b}}T$, $0 \leq \vartheta_{k,\mathrm{b}} \leq 1$, MU k scavenges energy from the ES's RF signals. Then, in the second phase with duration $(1 - \vartheta_{k,\mathrm{b}})T$, MU k utilizes the harvested energy to transmit data to the BS b_0. When MU k accesses SAP n, it switches between the HTT mode and the AB mode as shown in Fig. 3, where $\alpha_{k,n}$ and $\beta_{k,n}$, $0 \leq \alpha_{k,n}, \beta_{k,n} \leq T$, are time periods for the AB mode and the HTT mode of MU $k, \forall k \in \mathcal{K}$, respectively. Notice that if MU k is under the coverage of SAP n, but the distance between them is greater than the maximum distance $d^{\max}$, e.g., the above-mentioned 24 meters, to establish the AB communication for a specific transceiver design, then MU k can only work in the HTT mode, i.e., $\alpha_{k,n} = 0$.

B. Energy Consumption and Time Consumption

Each MU k can only access the BS b_0 or one of the SAPs for data transmission, that is, for MU k,

$$\sum_{n \in \mathcal{N}} y_{k,n} + y_{k,\mathrm{b}} \leq 1, \tag{1}$$

where $y_{k,\mathrm{b}} \in \{0,1\}$ and $y_{k,n} \in \{0,1\}, \forall n \in \mathcal{N}$. $y_{k,\mathrm{b}} = 1$ if MU k accesses the BS b_0; otherwise $y_{k,\mathrm{b}} = 0$. Similarly, $y_{k,n} = 1$ if MU k accesses SAP n; otherwise $y_{k,n} = 0$.

We assume that system channel state information (CSI) can be perfectly and also conveniently estimated because the BS b_0 (or SAP n) can send the training signals to the MUs, and then get the channel status feedback from the MUs to obtain CSI. Besides, the BS b_0, the SAPs, and the ES utilize different frequency bands, and thus there is no interference among them. Also, the MUs accessing the BS b_0 are allocated orthogonal spectrums, and we denote $s_{k,\mathrm{b}} \in [0,1]$ as the percentage of the BS b_0's spectrum allocated to MU k. Thus, we can express the

[1]As pointed out in [1], backscatter circuits are lightweight with low-power consumption, and thus they can be combined with hardware-constrained devices with low implementation complexity. In general, only a load modulator needs to be integrated into the RF front-end. Then, by switching between different load impedances and adapting the antenna's reflection coefficient, the backscatter node can modulate its information signals on the reflected signals [17].

[2]The MUs we consider are EH-based and low-power devices, e.g., wireless sensors, whose task data sizes are generally small. Therefore, it is practically feasible to utilize the low-rate and low-energy-consumption backscatter communications for traffic-offloading. Moreover, the authors of [7] have developed a novel AB communication system, i.e., BackFi, which can achieve a backscatter rate of 1 Mbps at a range of 5 meters. This further justifies the feasibility of using the backscatter communications for traffic-offloading. Furthermore, using the backscatter communications for traffic-offloading, the energy consumption of the EH-based MUs can be significantly reduced as shown in Section V.

Authorized licensed use limited to: Texas A M University. Downloaded on January 17,2022 at 20:42:04 UTC from IEEE Xplore. Restrictions apply.

achievable rate from MU k to the BS b_0, denoted by $R_{k,\mathrm{b}}$, as:

$$R_{k,\mathrm{b}} = s_{k,\mathrm{b}} W_\mathrm{b} \log_2 \left(1 + \frac{P_{k,\mathrm{b}} |h_{k,\mathrm{b}}|^2}{\zeta_k N_0}\right), \tag{2}$$

where ζ_k is a parameter related to the modulation and coding schemes, which is introduced to measure the signal-to-interference-plus-noise ratio (SINR) gap between MU k's achievable rate $R_{k,\mathrm{b}}$ and the channel capacity from MU k to the BS b_0 [26]–[29]. Besides, $h_{k,\mathrm{b}}$ and $P_{k,\mathrm{b}}$ are the channel gain and the transmit power from MU k to the BS b_0, respectively, N_0 is the noise power, and W_b denotes the bandwidth of the BS b_0. Hence, when the achievable rate $R_{k,\mathrm{b}} > 0$, i.e., $y_{k,\mathrm{b}} = 1$, we can write MU k's data transmission time, denoted by $T_{k,\mathrm{b}}$, and energy consumption, denoted by $E_{k,\mathrm{b}}$, as:

$$\begin{cases} T_{k,\mathrm{b}} = \frac{D_k}{R_{k,\mathrm{b}}}, & (3) \\ E_{k,\mathrm{b}} = P_{k,\mathrm{b}} T_{k,\mathrm{b}}, & (4) \end{cases}$$

respectively, where D_k is the data size of the task which needs to be transmitted by MU k.

Moreover, we assume that the spectrum assigned to the SAPs is divided into orthogonal subchannels. Each SAP is allocated one subchannel, and different SAPs can share the same subchannels to improve spectrum efficiency. However, to reduce inter-cell interference, adjacent SAPs are allocated different subchannels as much as possible. Besides, for a given SAP n, the MUs accessing it employ the TDMA technique to transmit data as shown in Fig. 3. Then, similar to [18], we can express the instantaneous achievable rate from MU k to SAP n, denoted by $R_{k,n}$, in the HTT mode when $y_{k,n} = 1$ as:

$$R_{k,n} = W_n \log_2 \left(1 + \frac{P_{k,n}|h_{k,n}|^2}{\zeta_k \left(N_0 + \sum_{n' \in \mathcal{I}_n} I_{n',n}\right)}\right), \tag{5}$$

where W_n is the bandwidth of SAP n, and $P_{k,n}$ and $h_{k,n}$ are the transmit power and the channel gain from MU k to SAP n, respectively, in the HTT mode. In addition, $\mathcal{I}_n$ is the set of SAPs which share the same subchannel with SAP n, and $I_{n',n}$ is the instantaneous interference to SAP n from MUs accessing SAP n'. MUs access SAP n' in a TDMA manner, and then $I_{n',n}$ may change with time during the data transmission period, i.e., $\beta_{k,n}$, of MU k in the HTT mode. Hence, if $Z_{k,n}$ bits of data are to be transmitted using the HTT mode when $y_{k,n} = 1$ and $\beta_{k,n} > 0$, we can obtain that the average achievable rate from MU k to SAP n satisfies the following equation.

$$\begin{aligned} \mathbb{E}\left[R_{k,n}\right] &= \mathbb{E}\left[W_n \log_2 \left(1 + \frac{P_{k,n}|h_{k,n}|^2}{\zeta_k \left(N_0 + \sum_{n' \in \mathcal{I}_n} I_{n',n}\right)}\right)\right] \\ &= \frac{Z_{k,n}}{\beta_{k,n}}. \end{aligned} \tag{6}$$

To obtain the energy consumption of MU k, denoted by $E_{k,n} \triangleq P_{k,n}\beta_{k,n}$, based on Eq. (6), we first give the following lemma.

Lemma 1: Let X and Y be non-negative and independent random variables such that $\mathbb{E}[X] < \infty$ and $\mathbb{E}[Y] < \infty$. Then,

$$\mathbb{E}_{X,Y}\left[\log_2\left(1 + \frac{X}{Y}\right)\right] \geq \mathbb{E}_X\left[\log_2\left(1 + \frac{X}{\mathbb{E}[Y]}\right)\right]. \tag{7}$$

Proof: Please see [30] and references therein. ∎

Since $P_{k,n}$ is a constant during the time period $\beta_{k,n}$, based on Eq. (6) and Lemma 1, we can obtain the following inequality.

$$\mathbb{E}\left[R_{k,n}\right] \geq W_n \log_2 \left(1 + \frac{P_{k,n}|h_{k,n}|^2}{\zeta_k \left(N_0 + \sum_{n' \in \mathcal{I}_n} \mathbb{E}\left[I_{n',n}\right]\right)}\right). \tag{8}$$

Utilizing Eq. (8) and $\mathbb{E}[R_{k,n}] = Z_{k,n}/\beta_{k,n}$ given in Eq. (6), we can obtain that

$$\begin{aligned} E_{k,n} &= P_{k,n}\beta_{k,n} \\ &\leq \frac{\beta_{k,n}\zeta_k \left(N_0 + \sum_{n' \in \mathcal{I}_n} \mathbb{E}\left[I_{n',n}\right]\right)}{|h_{k,n}|^2} f\left(\frac{Z_{k,n}}{\beta_{k,n} W_n}\right), \end{aligned} \tag{9}$$

when $\beta_{k,n} > 0$, where $f(x) \triangleq (2^x - 1)$. If $\beta_{k,n} = 0$ and $Z_{k,n} = 0$, we can define $E_{k,n} = 0$, since no data will be transmitted through the HTT mode when $Z_{k,n} = 0$. Moreover, when $\beta_{k,n} = 0$ and $Z_{k,n} > 0$, since

$$\begin{aligned} \lim_{\beta_{k,n} \to 0^+} & \frac{\beta_{k,n}\zeta_k \left(N_0 + \sum_{n' \in \mathcal{I}_n} \mathbb{E}\left[I_{n',n}\right]\right)}{|h_{k,n}|^2} f\left(\frac{Z_{k,n}}{\beta_{k,n} W_n}\right) \\ &= +\infty, \end{aligned} \tag{10}$$

we can define $E_{k,n}$ as a value which is larger than the maximum capacity $E_k^{\max}$ of MU k's energy storage. In this case, MU k cannot finish transmitting all its data by accessing SAP n, and then $y_{k,n} = 0$. Notice that when calculating $E_{k,n}$, we omit the small amount of energy used in the AB mode similar to [1]. This is because compared with the high power consumption of the active radio transmission in the HTT mode, the power consumption of the passive radio transmission in the AB mode is extremely low (typically a few μW) [1]–[3].

As mentioned above, the backscatter rate in the AB mode depends on the specific design of the backscatter transceiver [17]. Hence, similar to [1]–[8], we assume that the achievable backscatter rate B_k at MU k can be obtained in advance, and only takes the achievable backscatter rates realized by the AB hardware prototypes as developed in the existing literatures, e.g., [3], [4], [7]. Specifically, the backscatter rates reported in [3], [4], [7] are measured through real testing experiments using the developed AB hardware prototypes under different conditions, e.g., different distances between the backscatter transceivers. Then, when $y_{k,n} = 1$, the total time consumption of MU k for transmitting D_k bits of data to SAP n, denoted by $T_{k,n}$, is

$$T_{k,n} = \alpha_{k,n} + \beta_{k,n} = \frac{D_k - Z_{k,n}}{B_k} + \beta_{k,n}, \tag{11}$$

where $\alpha_{k,n} = (D_k - Z_{k,n})/B_k$ is the time consumption of MU k for data backscattering. Thus, once we determine $Z_{k,n}$, we can obtain $\alpha_{k,n}$.

C. Harvested Energy

Each MU k is equipped with a single antenna, and then it cannot harvest energy when transmitting or backscattering data. The practical RF-based EH circuits exhibit the non-linear characteristics of the end-to-end wireless energy transfer (WPT),

Authorized licensed use limited to: Texas A M University. Downloaded on January 17,2022 at 20:42:04 UTC from IEEE Xplore. Restrictions apply.

where the RF energy conversion efficiency changes with the received RF power level at MU k [31], [32]. Consequently, adopting the non-linear EH model developed in [32], when MU k accesses the BS b_0, we can express the harvested energy at MU k, denoted by $E^{\mathrm{h}}_{k,\mathrm{b}}$, as follows:

$$E^{\mathrm{h}}_{k,\mathrm{b}} = \left[\frac{\Phi_k \left(P_{\mathrm{e}} |h_{\mathrm{e},k}|^2 \right) - M_k \Omega_k}{1 - \Omega_k} \right] \vartheta_{k,\mathrm{b}} T, \tag{12}$$

where $\Phi_k(x) \triangleq M_k \ (1 + \exp\{-c_k(x - d_k)\})$, where M_k is the maximum harvested power when the EH circuit saturates, and c_k and d_k are positive constants relating to the EH circuit specification [32]. Moreover, $P_{\mathrm{e}}|h_{\mathrm{e},k}|^2$ is the received power level at MU k, where P_{e} is the transmit power of the ES and $h_{\mathrm{e},k}$ is the channel gain from the ES to MU k. In addition, $\Omega_k = 1 \ (1 + \exp\{c_k d_k\})$ is a constant to ensure zero-input zeros-output response for energy harvesting. To activate the EH circuit at MU k, the inequality $P_{\mathrm{e}}|h_{\mathrm{e},k}|^2 \geq d_k$ must hold, since d_k is related to the turn-on threshold of the diode in the EH circuits [32].

Similarly, we can express the harvested energy at MU k when accessing SAP n, denoted by $E^{\mathrm{h}}_{k,n}$, as:

$$\begin{aligned} E^{\mathrm{h}}_{k,n} = & \left[\frac{\Phi_k \left(P_{\mathrm{e}} |h_{\mathrm{e},k}|^2 \right) - M_k \Omega_k}{1 - \Omega_k} \right] \\ & \times \left(\sum_{k' \neq k} \frac{D_{k'} - Z_{k',n}}{B_{k'}} + \sum_{k' < k} \beta_{k',n} \right), \end{aligned} \tag{13}$$

where we omit the energy harvested in the AB mode, since the amount of energy harvested in the AB mode is relatively small, which is just sufficient to sustain backscatter operations of the MUs but cannot support the active radio transmission in the HTT mode [1]. Without loss of generality, we assume that MUs access SAP n one by one in a predefined order as shown in Fig. 3. Besides, since $\alpha_{k',n} = \beta_{k',n} = 0$ when $y_{k',n} = 0$, we can define $Z_{k',n} = D_{k'}$ for MU k' when $y_{k',n} = 0$ in Eq. (13).

III. Joint Optimization for Offloading and Resource-Allocation

A. Joint Optimization Problem Formulation

For the considered RF-powered mobile networks using the AB communication, we aim to minimize the total energy consumption of all EH-based MUs, by jointly optimizing all MUs' network access and system resource-allocation. Specifically, when $\beta_{k,n} > 0$, we will use the right hand side of Eq. (9) to calculate the energy consumption $E_{k,n}$ of MU k when it accesses SAP n. Thus, in fact, we aim to minimize the maximum energy consumption of all MUs in this paper. Hence, we can formulate the considered optimization problem as follows:

$$\min_{\boldsymbol{\psi}_{\mathrm{b}}, \{\boldsymbol{\psi}_n\}_{n \in \mathcal{N}}} \left(E_{\mathrm{b}} + \sum_{n \in \mathcal{N}} E_n \right) \tag{14}$$

s.t.

$$C1: \ y_{k,\mathrm{b}} \left(\vartheta_{k,\mathrm{b}} T + T_{k,\mathrm{b}} \right) \leq T, \forall k,$$

$$C2: \ \sum_{k \in \mathcal{K}} y_{k,n} T_{k,n} \leq T, \forall n,$$

$$C3: \ y_{k,\mathrm{b}} \left(E_{k,\mathrm{b}} + P_{\mathrm{c}} T_{k,\mathrm{b}} \right) \leq \min \left\{ E^{\mathrm{h}}_{k,\mathrm{b}}, E^{\max}_k \right\}, \forall k,$$

$$C4: \ y_{k,n} \left(E_{k,n} + P_{\mathrm{c}} \beta_{k,n} \right) \leq \min \left\{ E^{\mathrm{h}}_{k,n}, E^{\max}_k \right\}, \forall k, n,$$

$$C5: \ P_{k,\mathrm{b}} \leq y_{k,\mathrm{b}} P^{\max}_k, \forall k,$$

$$C6: \ P_{k,n} \leq y_{k,n} P^{\max}_k, \forall k, n,$$

$$C7: \ s_{k,\mathrm{b}} \leq y_{k,\mathrm{b}}, \forall k,$$

$$C8: \ \sum_{k \in \mathcal{K}} s_{k,\mathrm{b}} \leq 1,$$

$$C9: \ \sum_{n \in \mathcal{N}} y_{k,n} + y_{k,\mathrm{b}} \leq 1, \forall k,$$

$$C10: \ \mathbb{1} \left(P_{\mathrm{e}} |h_{\mathrm{e},k}|^2 < d_k \right) y_{k,\mathrm{b}} = 0, \forall k,$$

$$C11: \ \mathbb{1} \left(P_{\mathrm{e}} |h_{\mathrm{e},k}|^2 < d_k \right) \beta_{k,n} = 0, \forall k, n,$$

where $\mathbb{1}(\cdot)$ is the indicator function,[3]

$$\begin{cases} E_{\mathrm{b}} \triangleq \sum_{k \in \mathcal{K}} y_{k,\mathrm{b}} E_{k,\mathrm{b}}, & (15) \\ E_n \triangleq \sum_{k \in \mathcal{K}} y_{k,n} E_{k,n}, \forall n, & (16) \end{cases}$$

are the totally consumed energy of MUs accessing the BS b_0 and SAP n, respectively, and $\boldsymbol{\psi}_{\mathrm{b}} \triangleq \{\boldsymbol{\vartheta}_{\mathrm{b}}, \mathcal{S}_{\mathrm{b}}, \mathcal{P}_{\mathrm{b}}, \mathcal{Y}_{\mathrm{b}}\}$ and $\boldsymbol{\psi}_n \triangleq \{\mathcal{Z}_n, \boldsymbol{\beta}_n, \mathcal{P}_n, \mathcal{Y}_n\}, \forall n$, where

$$\begin{cases} \boldsymbol{\vartheta}_{\mathrm{b}} \triangleq \left\{ \vartheta_{k,\mathrm{b}} \in [0,1], \forall k \right\}, \\ \mathcal{S}_{\mathrm{b}} \triangleq \left\{ s_{k,\mathrm{b}} \in [0,1], \forall k \right\}, \\ \mathcal{P}_{\mathrm{b}} \triangleq \left\{ P_{k,\mathrm{b}} \in [0, P^{\max}_k], \forall k \right\}, \\ \mathcal{Y}_{\mathrm{b}} \triangleq \left\{ y_{k,\mathrm{b}} \in \{0,1\}, \forall k \right\}, \\ \mathcal{Z}_n \triangleq \left\{ Z_{k,n} \in [0, D_k], \forall k \right\}, \forall n, \\ \boldsymbol{\beta}_n \triangleq \left\{ \beta_{k,n} \in [0, T], \forall k \right\}, \forall n, \\ \mathcal{P}_n \triangleq \left\{ P_{k,n} \in [0, P^{\max}_k], \forall k \right\}, \forall n, \\ \mathcal{Y}_n \triangleq \left\{ y_{k,n} \in \{0,1\}, \forall k \right\}, \forall n. \end{cases}$$

Moreover, P_{c} is the constant circuit energy consumption when MU k working in the HTT mode, and $E^{\max}_k$ is the maximum capacity of MU k's energy storage. $C1 - C2$ are the time consumption constraints of MUs when accessing the BS b_0 and SAP n, respectively, which state that each MU should finish data transmission within T. $C3 - C4$ are the energy consumption constraints of MU k when accessing the BS b_0 and SAP n, respectively, which guarantee that the totally consumed energy of MU k cannot exceed the amount of the available energy in its energy storage. $C5 - C6$ are the power consumption constraints of MU k, where $P^{\max}_k$ is the maximum transmit power of MU k. $C7 - C8$ are the spectrum allocation constraints of the BS

[3]In the problem given in Eq. (14), since MU k's information cannot be sent to the BS b_0 when $y_{k,\mathrm{b}} = 0$, we define $T_{k,\mathrm{b}} = 0$ and $\vartheta_{k,\mathrm{b}} = 1$ when $y_{k,\mathrm{b}} = 0$. Correspondingly, we define $E_{k,\mathrm{b}}$ as a valued variable which is larger than $E^{\max}_k$ when $y_{k,n} = 0$. Similarly, we define $T_{k,n} = 0$ (i.e., $\alpha_{k,n} = \beta_{k,n} = 0$), and let $E_{k,\mathrm{b}}$ be a valued variable which is larger than $E^{\max}_k$ as mentioned in Section II-B. Moreover, for ease of mathematical tractability, we can still utilize Eqs. (12), (13) to calculate MU k's harvested energy, i.e., $E^{\mathrm{h}}_{k,\mathrm{b}}$ and $E^{\mathrm{h}}_{k,n}$, when $y_{k,\mathrm{b}} = 0$ and $y_{k,n} = 0$, respectively. Observing $C3 - C4$, we can know that this will not affect the solution to the problem in Eq. (14).

Authorized licensed use limited to: Texas A M University. Downloaded on January 17,2022 at 20:42:04 UTC from IEEE Xplore. Restrictions apply.

b_0, which ensure that only MUs accessing the BS b_0 can be allocated a part of the BS b_0's spectrum. $C9$ guarantees that MU k can only access the BS b_0 or one of the SAPs. Since d_k is related to the turn-on threshold of the diode in the EH circuits [32], $C10 - C11$ guarantee that if the received power level, i.e., $P_{\rm e}|h_{{\rm e},k}|^2$, at MU k from the ES is less than d_k, MU k cannot access the BS b_0. In this case, MU k can only choose to access one SAP n by working under the AB mode, i.e., $\beta_{k,n} = 0$.

B. Distributed Joint Traffic-Offloading and Resource-Allocation Optimization Schemes

The number of variables in the problem given in Eq. (14) will become extremely large for large-size mobile networks, which have a large number of MUs and/or SAPs. Hence, we need to solve the problem in Eq. (14) in a distributed way, by decomposing it into several subproblems. Since $y_{k,\rm b}$ and $y_{k,n}$'s are coupled in $C9$ for MU k, similar to [33], [34], we use the alternating directions method of multipliers (ADMM) to decompose the problem in Eq. (14) into several subproblems, with each corresponding to one SAP or the BS b_0.[4] Notice that due to taking into account the inter-cell interference among SAPs sharing the same subchannels, the upper-bound of $E_{k,n}$, i.e., the right hand of Eq. (9), becomes a non-convex function and thus the minimization problem given by Eq. (14) becomes a non-convex optimization problem. While the ADMM technique is usually often used to solve the convex optimization problems, as shown and actually applied in [34], [36], [37], ADMM can be also employed to solve the non-convex optimization problems. As a result, we can still apply the ADMM method to solve our non-convex optimization problem given by Eq. (14). To apply ADMM, we first introduce copies of $y_{k,\rm b}$'s and $y_{k,n}$'s, and define them as $\widehat{y}_{k,\rm b}$'s and $\widehat{y}_{k,n}$'s, respectively. Then, we have

$$\begin{cases} C12: & \widehat{y}_{k,\rm b} = y_{k,\rm b}, \quad \forall k, \\ C13: & \widehat{y}_{k,n} = y_{k,n}, \quad \forall k, n. \end{cases}$$

Furthermore, the constraint $C9$ can be rewritten as:

$$C14: \sum_{n\in\mathcal{N}} \widehat{y}_{k,n} + \widehat{y}_{k,\rm b} \le 1, \forall k.$$

Based on $C12 - C14$, we can reformulate the optimization problem given in Eq. (14) as follows:

$$\min_{\widehat{\mathcal{Y}}_{\rm b},\boldsymbol{\psi}_{\rm b},\left\{\widehat{\mathcal{Y}}_n,\boldsymbol{\psi}_n\right\}_{n\in\mathcal{N}}} \left(E_{\rm b} + \sum_{n\in\mathcal{N}} E_n\right) \tag{17}$$
$$\textbf{s.t.} \quad C1 - C8, C10 - C11, C12 - C14,$$

where $\widehat{\mathcal{Y}}_{\rm b} \triangleq \{\widehat{y}_{k,\rm b} \in \{0,1\}, \forall k\}$ and $\widehat{\mathcal{Y}}_n \triangleq \{\widehat{y}_{k,n} \in \{0,1\}, \forall k\}$, $\forall n$. Then, according to [34], the augmented Lagrangian function of the problem specified by Eq. (17) can be given by:

$$\begin{aligned} &\mathcal{L}\left(\widehat{\mathcal{Y}}_{\rm b},\boldsymbol{\psi}_{\rm b},\left\{\widehat{\mathcal{Y}}_n,\boldsymbol{\psi}_n\right\}_{n\in\mathcal{N}},\boldsymbol{\Lambda}\right) \\ &= E_{\rm b} + \sum_{n\in\mathcal{N}} E_n \\ &\quad + \sum_{n\in\mathcal{N}}\sum_{k\in\mathcal{K}} \mu_{k,n}\left(y_{k,n} - \widehat{y}_{k,n}\right) + \sum_{k\in\mathcal{K}} \lambda_k \left(y_{k,\rm b} - \widehat{y}_{k,\rm b}\right) \\ &\quad + \frac{\rho}{2}\sum_{n\in\mathcal{N}}\sum_{k\in\mathcal{K}} \left(y_{k,n} - \widehat{y}_{k,n}\right)^2 + \frac{\rho}{2}\sum_{k\in\mathcal{K}} \left(y_{k,\rm b} - \widehat{y}_{k,\rm b}\right)^2, \end{aligned} \tag{18}$$

and correspondingly the dual function and the dual problem of the problem given in Eq. (17) are, respectively, given by:

$$d(\boldsymbol{\Lambda}) \triangleq \min_{\widehat{\mathcal{Y}}_{\rm b},\boldsymbol{\psi}_{\rm b},\left\{\widehat{\mathcal{Y}}_n,\boldsymbol{\psi}_n\right\}_{n\in\mathcal{N}}} \mathcal{L}\left(\widehat{\mathcal{Y}}_{\rm b},\boldsymbol{\psi}_{\rm b},\left\{\widehat{\mathcal{Y}}_n,\boldsymbol{\psi}_n\right\}_{n\in\mathcal{N}},\boldsymbol{\Lambda}\right), \tag{19}$$
$$\textbf{s.t.} \quad C1 - C8, C10 - C11, C14,$$

and

$$\max_{\boldsymbol{\Lambda}} \left\{d(\boldsymbol{\Lambda})\right\}, \tag{20}$$

where $\boldsymbol{\Lambda} \triangleq \{\lambda_k, \mu_{k,n}, \forall k, n\}$ is the set of Lagrange multipliers associated with $C12 - C13$. $\rho > 0$ is the penalty parameter, which is a constant parameter to control the convergence speed of ADMM [34]. Besides, for any feasible solution to the problem specified by Eq. (17), the ρ-terms in Eq. (18) are actually equal to zero [36]–[38].

We use τ to denote the iteration index of the ADMM method, when solving the problem given in Eq. (17). Applying ADMM, we can describe the resulting optimization steps as follows:

1) Updating Variables $\boldsymbol{\psi}_b$ and $\boldsymbol{\psi}_n$, $\forall n$: Given $\widehat{\mathcal{Y}}_{\rm b}^{[\tau]}$, $\widehat{\mathcal{Y}}_n^{[\tau]}$, $\forall n$, and $\boldsymbol{\Lambda}^{[\tau]}$, we derive $\boldsymbol{\psi}_{\rm b}^{[\tau+1]}$ and $\boldsymbol{\psi}_n^{[\tau+1]}$, $\forall n$, by solving the problem in Eq. (18), where $x^{[\tau]}$ is the obtained x in the $(\tau-1)$th iteration of the ADMM method. That is, we solve the following problem:

$$\min_{\boldsymbol{\psi}_{\rm b},\{\boldsymbol{\psi}_n\}_{n\in\mathcal{N}}} \mathcal{L}\left(\widehat{\mathcal{Y}}_{\rm b}^{[\tau]},\boldsymbol{\psi}_{\rm b},\left\{\widehat{\mathcal{Y}}_n^{[\tau]},\boldsymbol{\psi}_n\right\}_{n\in\mathcal{N}},\boldsymbol{\Lambda}^{[\tau]}\right) \tag{21}$$
$$\textbf{s.t.} \quad C1 - C8, C10 - C11.$$

Observing Eq. (18), due to the introduction of variables $\widehat{y}_{k,\rm b}$'s and $\widehat{y}_{k,n}$'s, we can decompose the optimization problem given in Eq. (21) into the following $(N+1)$ parallel subproblems. For the BS b_0, the subproblem is:

$$\min_{\boldsymbol{\psi}_{\rm b}} \mathcal{L}_{\rm b}\left(\widehat{\mathcal{Y}}_{\rm b}^{[\tau]},\boldsymbol{\psi}_{\rm b},\boldsymbol{\Lambda}^{[\tau]}\right) \tag{22}$$
$$\textbf{s.t.} \quad C1, C3, C5, C7 - C8, C10,$$

and for SAP n, $\forall n \in \mathcal{N}$, the subproblem is:

$$\min_{\boldsymbol{\psi}_n} \mathcal{L}_n\left(\widehat{\mathcal{Y}}_n^{[\tau]},\boldsymbol{\psi}_n,\boldsymbol{\Lambda}^{[\tau]}\right) \tag{23}$$
$$\textbf{s.t.} \quad C2, C4, C6, C11,$$

[4] There are several other distributed algorithms which can be used to solve the optimization problem in Eq. (14). The numerical results in Section V show that the performance of ADMM is not worse than that of the other distributed algorithms, e.g., the successive upper bound minimization (BSUM) method [35]. Hence, we apply ADMM to solve the optimization problem given by Eq. (14).

Authorized licensed use limited to: Texas A M University. Downloaded on January 17,2022 at 20:42:04 UTC from IEEE Xplore. Restrictions apply.

where

$$\begin{cases} \mathcal{L}_{\rm b}\left(\widehat{\mathcal{Y}}_{\rm b}^{[\tau]}, \boldsymbol{\psi}_{\rm b}, \boldsymbol{\Lambda}^{[\tau]}\right) = E_{\rm b} + \sum_{k\in\mathcal{K}} \lambda_k^{[\tau]}\left(y_{k,{\rm b}} - \widehat{y}_{k,{\rm b}}^{[\tau]}\right) \\ \qquad\qquad + \frac{\rho}{2}\sum_{k\in\mathcal{K}}\left(y_{k,{\rm b}} - \widehat{y}_{k,{\rm b}}^{[\tau]}\right)^2, & (24) \\ \mathcal{L}_n\left(\widehat{\mathcal{Y}}_n^{[\tau]}, \boldsymbol{\psi}_n, \boldsymbol{\Lambda}^{[\tau]}\right) = E_n + \sum_{k\in\mathcal{K}} \mu_{k,n}^{[\tau]}\left(y_{k,n} - \widehat{y}_{k,n}^{[\tau]}\right) \\ \qquad\qquad + \frac{\rho}{2}\sum_{k\in\mathcal{K}}\left(y_{k,n} - \widehat{y}_{k,n}^{[\tau]}\right)^2. & (25) \end{cases}$$

The problems given in Eqs. (22)–(23), which can be solved by the BS b_0 and SAP n, $n \in \mathcal{N}$, respectively, are non-convex optimization problems, due to the product terms, e.g., $y_{k,n}\beta_{k,n}$, $\forall k, n$, the integer variables $y_{k,{\rm b}}$'s, etc. When solving the problem given in Eq. (22), we first denote $\mathcal{U} \triangleq \{k|, P_{\rm e}|h_{{\rm e},k}|^2 \geq d_k, \forall k \in \mathcal{K}\}$. Due to $C10$, the BS b_0 can only serve MUs in the set $\mathcal{U}$, and then it can directly set $y_{k,{\rm b}} = 0$ if $k \notin \mathcal{U}$ and only solve the problem in Eq. (22) for MUs in $\mathcal{U}$. If MU k, $\forall k \in \mathcal{U}$, accesses the BS b_0, then to minimize MU k's energy consumption, it is obvious that the following equation must hold seen from C1.

$$T_{k,{\rm b}} = (1 - \vartheta_{k,{\rm b}})\,T, \tag{26}$$

which indicates that in each time slot, after energy harvesting, MU k accessing the BS b_0 should spend all the remaining time with duration $(1 - \vartheta_{k,{\rm b}})T$ for data transmission.[5]

Plugging $T_{k,{\rm b}}, \forall k \in \mathcal{U}$, given in Eq. (26) into $E_{k,{\rm b}} = P_{k,{\rm b}}T_{k,{\rm b}}$ (see Eq. (4)), and $E_{\rm b} = \sum_{k\in\mathcal{K}} y_{k,{\rm b}}E_{k,{\rm b}}$ (see Eq. (15)), we can rewrite C3 and $\mathcal{L}_{\rm b}(\widehat{\mathcal{Y}}_{\rm b}^{[\tau]}, \boldsymbol{\psi}_{\rm b}, \boldsymbol{\Lambda}^{[\tau]})$ given in Eq. (24), respectively, as follows:

$$y_{k,{\rm b}}P_{k,{\rm b}}(1 - \vartheta_{k,{\rm b}})T + y_{k,{\rm b}}P_{\rm c}(1 - \vartheta_{k,{\rm b}})T \leq E_{k,{\rm b}}^{\rm h}, \forall k \in \mathcal{U}, \tag{27}$$

and

$$\begin{aligned} &\mathcal{L}_{\rm b}\left(\widehat{\mathcal{Y}}_{\rm b}^{[\tau]}, \boldsymbol{\psi}_{\rm b}, \boldsymbol{\Lambda}^{[\tau]}\right) \\ &\quad = \sum_{k\in\mathcal{U}} y_{k,{\rm b}}P_{k,{\rm b}}(1 - \vartheta_{k,{\rm b}})T + \sum_{k\in\mathcal{U}} \lambda_k^{[\tau]}\left(y_{k,{\rm b}} - \widehat{y}_{k,{\rm b}}^{[\tau]}\right) \\ &\quad + \frac{\rho}{2}\sum_{k\in\mathcal{U}}\left(y_{k,{\rm b}} - \widehat{y}_{k,{\rm b}}^{[\tau]}\right)^2. \end{aligned} \tag{28}$$

Moreover, using Eq. (2) and the expressions of $T_{k,{\rm b}}$ in Eqs. (3) and (26), for MU k, $\forall k \in \mathcal{U}$, we can get the following inequality, where we provide the detailed derivation in Appendix A.

$$\frac{y_{k,{\rm b}}}{(1 - \vartheta_{k,{\rm b}})T} \leq \frac{1}{D_k}\left[s_{k,{\rm b}}W_{\rm b}\log_2\left(1 + \frac{y_{k,{\rm b}}P_{k,{\rm b}}|h_{k,{\rm b}}|^2}{N_0}\right)\right], \tag{29}$$

where the equality holds when the problem specified by Eq. (22) attains the optimal solution.

Then, we can rewrite the problem given in Eq. (22) as:

$$\begin{aligned} &\min_{\boldsymbol{\psi}_{\rm b}} \mathcal{L}_{\rm b}\left(\widehat{\mathcal{Y}}_{\rm b}^{[\tau]}, \boldsymbol{\psi}_{\rm b}, \boldsymbol{\Lambda}^{[\tau]}\right) \\ &\textbf{s.t.} \quad C5, C7 - C8, \text{Eq.}(27), \text{Eq.}(29), \end{aligned} \tag{30}$$

where $\mathcal{L}_{\rm b}(\widehat{\mathcal{Y}}_{\rm b}^{[\tau]}, \boldsymbol{\psi}_{\rm b}, \boldsymbol{\Lambda}^{[\tau]})$ is given in Eq. (28). To solve the problem given in Eq. (30), we first utilize the reformulation linearization technique (RLT) method to deal with the product term $y_{k,{\rm b}}P_{k,{\rm b}}, \forall k \in \mathcal{U}$, in Eqs. (27)–(29). Introducing the following new variable:

$$\widetilde{P}_{k,{\rm b}} \triangleq y_{k,{\rm b}}P_{k,{\rm b}}, \forall k \in \mathcal{U}, \tag{31}$$

we can obtain the following theorem using the RLT.

Theorem 1: **If** the RLT is applied, **then** the variable $\widetilde{P}_{k,{\rm b}}$, $\forall k \in \mathcal{U}$, defined in Eq. (31) is equivalent to the following linear constraints.

$$\begin{cases} 0 \leq \widetilde{P}_{k,{\rm b}} \leq P_{k,{\rm b}}, \forall k \in \mathcal{U}, & (32) \\ \widetilde{P}_{k,{\rm b}} \geq P_k^{\max}y_{k,{\rm b}} + P_{k,{\rm b}} - P_k^{\max}, \forall k \in \mathcal{U}, & (33) \\ \widetilde{P}_{k,{\rm b}} \leq y_{k,{\rm b}}P_k^{\max}, \forall k \in \mathcal{U}. & (34) \end{cases}$$

Proof: The proof is provided in Appendix B. ■

For MU k, $k \in \mathcal{U}$, the introduction of $\widetilde{P}_{k,{\rm b}}$ allows us to rewrite Eqs. (27) and (29), respectively, as follows:

$$\begin{cases} \widetilde{P}_{k,{\rm b}}(1 - \vartheta_{k,{\rm b}})T + P_{\rm c}y_{k,{\rm b}}(1 - \vartheta_{k,{\rm b}})T \leq E_{k,{\rm b}}^{\rm h}, & (35) \\ \frac{y_{k,{\rm b}}}{(1-\vartheta_{k,{\rm b}})T} \leq \frac{1}{D_k}\left[s_{k,{\rm b}}W_{\rm b}\log_2\left(1 + \frac{\widetilde{P}_{k,{\rm b}}|h_{k,{\rm b}}|^2}{N_0}\right)\right]. & (36) \end{cases}$$

Also, we can rewrite $\mathcal{L}_{\rm b}(\widehat{\mathcal{Y}}_{\rm b}^{[\tau]}, \boldsymbol{\psi}_{\rm b}, \boldsymbol{\Lambda}^{[\tau]})$ in Eq. (28) as:

$$\begin{aligned} &\widetilde{\mathcal{L}}_{\rm b}\left(\widehat{\mathcal{Y}}_{\rm b}^{[\tau]}, \boldsymbol{\psi}_{\rm b}, \widetilde{\mathcal{P}}_{\rm b}, \boldsymbol{\Lambda}^{[\tau]}\right) \\ &\quad = \sum_{k\in\mathcal{U}} \widetilde{P}_{k,{\rm b}}(1 - \vartheta_{k,{\rm b}})T + \sum_{k\in\mathcal{U}} \lambda_k^{[\tau]}\left(y_{k,{\rm b}} - \widehat{y}_{k,{\rm b}}^{[\tau]}\right) \\ &\quad + \frac{\rho}{2}\sum_{k\in\mathcal{U}}\left(y_{k,{\rm b}} - \widehat{y}_{k,{\rm b}}^{[\tau]}\right)^2, \end{aligned} \tag{37}$$

where $\widetilde{\mathcal{P}}_{\rm b} \triangleq \{\widetilde{P}_{k,{\rm b}} \in [0, \widetilde{P}_k^{\max}], \forall k \in \mathcal{U}\}$.

Based on Theorem 1 and Eqs. (35)–(37), we can transform the problem given in Eq. (30) as the following problem:

$$\begin{aligned} &\min_{\boldsymbol{\psi}_{\rm b}, \widetilde{\mathcal{P}}_{\rm b}} \widetilde{\mathcal{L}}_{\rm b}\left(\widehat{\mathcal{Y}}_{\rm b}^{[\tau]}, \boldsymbol{\psi}_{\rm b}, \widetilde{\mathcal{P}}_{\rm b}, \boldsymbol{\Lambda}^{[\tau]}\right) \\ &\textbf{s.t.} \quad C5, C7 - C8, \text{Eqs.}(32) - (36). \end{aligned} \tag{38}$$

To solve the problem specified by Eq. (38), we relax $y_{k,{\rm b}}$ for MU k, $k \in \mathcal{U}$, to be a real-valued variable taking values within [0, 1], which can be interpreted as the time fraction of MU k in accessing the BS b_0 for data transmission [38]. We utilize the alternative optimization method to solve this problem iteratively. First, since $C5$, $C7 - C8$, and Eqs. (32)-(36) are all convex constraints, and the objective function is a convex function with respect to $\mathcal{P}_{\rm b}$, $\mathcal{Y}_{\rm b}$, and $\widetilde{\mathcal{P}}_{\rm b}$ for given $\mathcal{S}_{\rm b}$ and $\boldsymbol{\vartheta}_{\rm b}$, the problem in Eq. (38) is a convex optimization problem with respect to $\mathcal{P}_{\rm b}$, $\mathcal{Y}_{\rm b}$, and $\widetilde{\mathcal{P}}_{\rm b}$. Hence, we can solve it easily by using the standard convex optimization methods, e.g., the interior-point method [39]. Similarly, we can transform the problem in Eq. (38) as a convex optimization problem for given $\mathcal{P}_{\rm b}$, $\mathcal{Y}_{\rm b}$, and $\widetilde{\mathcal{P}}_{\rm b}$, and then to obtain $\mathcal{S}_{\rm b}$ and $\boldsymbol{\vartheta}_{\rm b}$. The above procedures repeat iteratively until $\boldsymbol{\vartheta}_{\rm b}$, $\mathcal{S}_{\rm b}$, $\mathcal{P}_{\rm b}$, $\mathcal{Y}_{\rm b}$, and $\widetilde{\mathcal{P}}_{\rm b}$ converge to $\boldsymbol{\vartheta}_{\rm b}^{[\tau+1]}$, $\mathcal{S}_{\rm b}^{[\tau+1]}$, $\mathcal{P}_{\rm b}^{[\tau+1]}$, $\mathcal{Y}_{\rm b}^{[\tau+1]}$, and $\widetilde{\mathcal{P}}_{\rm b}^{[\tau+1]}$, respectively, and then we can obtain $\boldsymbol{\psi}_{\rm b}^{[\tau+1]} \triangleq \{\boldsymbol{\vartheta}_{\rm b}^{[\tau+1]}, \mathcal{P}_{\rm b}^{[\tau+1]}, \mathcal{S}_{\rm b}^{[\tau+1]}, \mathcal{Y}_{\rm b}^{[\tau+1]}\}$.

[5]If MU k, $\forall k \in \mathcal{U}$, does not access the BS b_0, Eq. (26) still holds, since $T_{k,{\rm b}} = 0$ and $\vartheta_{k,{\rm b}} = 1$ as mentioned in Section III-A.

Authorized licensed use limited to: Texas A M University. Downloaded on January 17,2022 at 20:42:04 UTC from IEEE Xplore. Restrictions apply.

Now, we solve the problem given in Eq. (23) to obtain $\boldsymbol{\psi}_n^{[\tau+1]} \triangleq \{\mathcal{Z}_n^{[\tau+1]}, \boldsymbol{\beta}_n^{[\tau+1]}, \mathcal{P}_n^{[\tau+1]}, \mathcal{Y}_n^{[\tau+1]}\}$ for SAP n, $\forall n \in \mathcal{N}$. Denote $\mathcal{U}_n$ as the set of MUs which are under the coverage of SAP n. Due to $C11$, SAP n can directly set $\beta_{k,n}=0$, and then $Z_{k,n}=0$ and $E_{k,n}$=0 for MU k, $\forall k \in \mathcal{U}_n \setminus \mathcal{U}$. For MU k, $\forall k \in \mathcal{U}_n \cap \mathcal{U}$, since $y_{k,n} \in \{0,1\}$, assuming that $\beta_{k,n}>0$, and using the right hand side of Eq. (9) to calculate $E_{k,n}$, we can rewrite $y_{k,n}E_{k,n}$ in the problem given by Eq. (23) as follows:

$$\begin{aligned} y_{k,n}&E_{k,n} \\ &= \frac{y_{k,n}\beta_{k,n}\zeta_k\left(N_0+\sum_{n'\in\mathcal{I}_n}\mathbb{E}\left[I_{n',n}\right]\right)}{|h_{k,n}|^2} f\left(\frac{Z_{k,n}}{\beta_{k,n}W_n}\right) \\ &= \frac{\beta_{k,n}\zeta_k\left(N_0+\sum_{n'\in\mathcal{I}_n}\mathbb{E}\left[I_{n',n}\right]\right)}{|h_{k,n}|^2} f\left(\frac{y_{k,n}Z_{k,n}}{\beta_{k,n}W_n}\right), \quad (39)\end{aligned}$$

where to solve the N subproblems in Eq. (23) efficiently and in parallel, we approximate the average interference $\mathbb{E}[I_{n',n}]$ from SAP n', $\forall n' \in \mathcal{I}_n$, to SAP n by using the following equation:

$$\sum_{k\in\mathcal{U}_{n'}} \frac{y_{k,n'}^{[\tau]}\beta_{k,n'}^{[\tau]}}{\sum_{k'\in\mathcal{U}_{n'}} y_{k',n'}^{[\tau]}\beta_{k',n'}^{[\tau]}} P_{k,n'}^{[\tau]}|h_{k,n}|^2 \quad (40)$$

when $\sum_{k'\in\mathcal{U}_{n'}}\beta_{k',n'}^{[\tau]}>0$; otherwise we approximate $\mathbb{E}[I_{n',n}]$ as 0. Here, $y_{k,n'}^{[\tau]}$, $\beta_{k,n'}^{[\tau]}$, $y_{k',n'}^{[\tau]}$, $\beta_{k',n'}^{[\tau]}$, and $P_{k,n'}^{[\tau]}$, $\forall n' \in \mathcal{I}_n$, $k,k' \in \mathcal{U}_{n'}$, are obtained in the $(\tau-1)$th iteration of the ADMM method. Based on Eq. (40), SAP n can calculate $\mathbb{E}[I_{n',n}]$ by only using the local information, e.g., $y_{k,n'}^{[\tau]}$, $y_{k',n'}^{[\tau]}$, and $\beta_{k',n'}^{[\tau]}$, $\forall n' \in \mathcal{I}_n, k, k' \in \mathcal{U}_{n'}$, and the N SAPs can solve the N subproblems given by Eq. (23) in parallel. Then, plugging $T_{k,n}$ given in Eq. (11) into $C2$, and plugging $y_{k,n}E_{k,n}$ given in Eq. (39) into $C4$ and the function $\mathcal{L}_n(\widehat{\mathcal{Y}}_n^{[\tau]}, \boldsymbol{\psi}_n, \boldsymbol{\Lambda}^{[\tau]})$ (see Eq. (25)), for SAP n, we can rewrite the problem specified by Eq. (23) as the following optimization problem:

$$\min_{\boldsymbol{\psi}_n} \mathcal{L}_n\left(\widehat{\mathcal{Y}}_n^{[\tau]}, \boldsymbol{\psi}_n, \boldsymbol{\Lambda}^{[\tau]}\right) \quad (41)$$

$$\begin{aligned} \textbf{s.t.}\ & C6, \\ & \sum_{k\in\mathcal{U}_n} y_{k,n}\left(\frac{D_k - Z_{k,n}}{B_k}+\beta_{k,n}\right) \le T, \\ & \frac{\beta_{k,n}\zeta_k\left(N_0+\sum_{n'\in\mathcal{I}_n}\mathbb{E}\left[I_{n',n}\right]\right)}{|h_{k,n}|^2} f\left(\frac{y_{k,n}Z_{k,n}}{\beta_{k,n}W_n}\right) \\ & \quad + P_{\mathrm{c}}y_{k,n}\beta_{k,n} \le \min\left\{E_{k,n}^{\mathrm{h}}, E_k^{\max}\right\}, \forall k \in \mathcal{U}_n \cap \mathcal{U},\end{aligned}$$

where we only need to consider the energy consumption for MUs in $\mathcal{U}_n \cap \mathcal{U}$, and

$$\begin{aligned} \mathcal{L}_n&\left(\widehat{\mathcal{Y}}_n^{[\tau]}, \boldsymbol{\psi}_n, \boldsymbol{\Lambda}^{[\tau]}\right) \\ &= \sum_{k\in\mathcal{U}_n\cap\mathcal{U}} \frac{\beta_{k,n}\zeta_k\left(N_0+\sum_{n'\in\mathcal{I}_n}\mathbb{E}\left[I_{n',n}\right]\right)}{|h_{k,n}|^2} f\left(\frac{y_{k,n}Z_{k,n}}{\beta_{k,n}W_n}\right) \\ &\quad + \sum_{k\in\mathcal{U}_n}\mu_{k,n}^{[\tau]}\left(y_{k,n}-\widehat{y}_{k,n}^{[\tau]}\right) + \frac{\rho}{2}\sum_{k\in\mathcal{U}_n}\left(y_{k,n}-\widehat{y}_{k,n}^{[\tau]}\right)^2. \end{aligned} \quad (42)$$

For solving the optimization problem given in Eq. (41), we first utilize the RLT to deal with the product terms $y_{k,n}Z_{k,n}$ and $y_{k,n}\beta_{k,n}$, $\forall k \in \mathcal{U}_n$. Introducing the following new variables:

$$\begin{cases} \widetilde{Z}_{k,n} \triangleq y_{k,n}Z_{k,n}, \forall k \in \mathcal{U}_n, & (43) \\ \widetilde{\beta}_{k,n} \triangleq y_{k,n}\beta_{k,n}, \forall k \in \mathcal{U}_n, & (44) \end{cases}$$

similar to Theorem 1, we can obtain the following Theorem 2 by using the RLT and considering the fact that $y_{k,n} \in \{0,1\}$, $0 \le Z_{k,n} \le D_k$, and $0 < \beta_{k,n} \le T$, $\forall k \in \mathcal{U}_n$.

Theorem 2: **If** the RLT is applied, **then** the variables $\widetilde{Z}_{k,n}$'s and $\widetilde{\beta}_{k,n}$'s defined in Eqs. (43)-(44) are equivalent to the following equations in terms of linear constraints, respectively.

$$\begin{cases} 0 \le \widetilde{Z}_{k,n} \le Z_{k,n}, \forall k \in \mathcal{U}_n, & (45) \\ \widetilde{Z}_{k,n} \ge D_k y_{k,n} + Z_{k,n} - D_k, \forall k \in \mathcal{U}_n, & (46) \\ \widetilde{Z}_{k,n} \le D_k y_{k,n}, \forall k \in \mathcal{U}_n, & (47) \end{cases}$$

and

$$\begin{cases} 0 \le \widetilde{\beta}_{k,n} \le \beta_{k,n}, \forall k \in \mathcal{U}_n, & (48) \\ \widetilde{\beta}_{k,n} \ge T y_{k,n} + \beta_{k,n} - T, \forall k \in \mathcal{U}_n, & (49) \\ \widetilde{\beta}_{k,n} \le T y_{k,n}, \forall k \in \mathcal{U}_n. & (50) \end{cases}$$

Based on the definition of $\widetilde{Z}_{k,n}$'s and $\widetilde{\beta}_{k,n}$'s, and Theorem 2, we can transform the problem given in Eq. (41) as the following optimization problem:

$$\min_{\boldsymbol{\psi}_n, \widetilde{\mathcal{Z}}_n, \widetilde{\boldsymbol{\beta}}_n} \widetilde{\mathcal{L}}_n\left(\widehat{\mathcal{Y}}_n^{[\tau]}, \boldsymbol{\psi}_n, \boldsymbol{\Lambda}^{[\tau]}\right) \quad (51)$$

$$\begin{aligned} \textbf{s.t.}\ & C6, \text{Eqs.}(45)\text{–}(50), \\ & \sum_{k\in\mathcal{U}_n}\left(\frac{y_{k,n}D_k - \widetilde{Z}_{k,n}}{B_k}+\widetilde{\beta}_{k,n}\right) \le T, \\ & \frac{\beta_{k,n}\zeta_k\left(N_0+\sum_{n'\in\mathcal{I}_n}\mathbb{E}\left[I_{n',n}\right]\right)}{|h_{k,n}|^2} f\left(\frac{\widetilde{Z}_{k,n}}{\beta_{k,n}W_n}\right) \\ & \quad + P_{\mathrm{c}}\widetilde{\beta}_{k,n} \le \min\left\{E_{k,n}^{\mathrm{h}}, E_k^{\max}\right\}, \forall k \in \mathcal{U}_n \cap \mathcal{U},\end{aligned}$$

where for SAP n,

$$\begin{aligned} \widetilde{\mathcal{L}}_n&\left(\widehat{\mathcal{Y}}_n^{[\tau]}, \boldsymbol{\psi}_n, \boldsymbol{\Lambda}^{[\tau]}\right) \\ &= \sum_{k\in\mathcal{U}_n\cap\mathcal{U}} \frac{\beta_{k,n}\zeta_k\left(N_0+\sum_{n'\in\mathcal{I}_n}\mathbb{E}\left[I_{n',n}\right]\right)}{|h_{k,n}|^2} f\left(\frac{\widetilde{Z}_{k,n}}{\beta_{k,n}W_n}\right) \\ &\quad + \sum_{k\in\mathcal{U}_n}\mu_{k,n}^{[\tau]}\left(y_{k,n}-\widehat{y}_{k,n}^{[\tau]}\right) + \frac{\rho}{2}\sum_{k\in\mathcal{U}_n}\left(y_{k,n}-\widehat{y}_{k,n}^{[\tau]}\right)^2 \end{aligned} \quad (52)$$

and

$$\begin{cases} \widetilde{\mathcal{Z}}_n \triangleq \left\{\widetilde{Z}_{k,n} \in [0, D_k], \forall k \in \mathcal{U}_n\right\}, \\ \widetilde{\boldsymbol{\beta}}_n \triangleq \left\{\widetilde{\beta}_{k,n} \in [0, T], \forall k \in \mathcal{U}_n\right\}. \end{cases}$$

Since $f(\widetilde{Z}_{k,n}) = N_0(2^{\widetilde{Z}_{k,n}}-1)$ is a convex function with respect to $\widetilde{Z}_{k,n}$, its perspective function $\beta_{k,n}f(\widetilde{Z}_{k,n}/(\beta_{k,n}W_n))$ is jointly convex with respect to $\beta_{k,n}$ and $\widetilde{Z}_{k,n}$ [39]. For MU

Authorized licensed use limited to: Texas A M University. Downloaded on January 17,2022 at 20:42:04 UTC from IEEE Xplore. Restrictions apply.

k, $\forall k \in \mathcal{U}_n$, relaxing $y_{k,n}$ to be a real-valued variable taking values within $[0,1]$, we can transform the problem specified by Eq. (51) as a convex optimization problem, where the relaxed variable $y_{k,n}$ can be interpreted as the time fraction of MU k in accessing SAP n for data transmission. Besides, please notice that when transforming the problem given in Eq. (23) as the problem given in Eq. (51), we assume that $\beta_{k,n} > 0$ for MU k, $\forall k \in \mathcal{U}_n \cap \mathcal{U}$, and rewrite $y_{k,n}E_{k,n}$ in the problem given in Eq. (23) as Eq. (39). However, when MU k accesses SAP n, i.e., $y_{k,n} = 1$, but $Z_{k,n} = 0$, MU k's data transmission time $\beta_{k,n} = 0$ and energy consumption $E_{k,n} = 0$. Moreover, when MU k does not access SAP n, i.e., $y_{k,n} = 0$, the variable $\beta_{k,n} = 0$ and the energy consumption $E_{k,n}$ can be defined as a value which is larger than $E_k^{\max}$. We can approximate the above two cases using the obtained solution to the problem given in Eq. (51). For example, when the obtained $\beta_{k,n} > 0$ but $Z_{k,n} = 0$, we can set $\beta_{k,n} = 0$ and $E_{k,n} = 0$ for MU k. When the obtained $\beta_{k,n} > 0$ and $Z_{k,n} > 0$, but $E_{k,n} > E_k^{\max}$, we can set $\beta_{k,n} = 0$ and $y_{k,n} = 0$, then $y_{k,n}E_{k,n} = 0$.

2) Updating Variables $\widehat{\mathcal{Y}}_b$ and $\widehat{\mathcal{Y}}_n$, $\forall n$: Given $\mathbf{\Lambda}^{[\tau]}$, and the above-obtained $\boldsymbol{\psi}_{\rm b}^{[\tau+1]}$ and $\boldsymbol{\psi}_n^{[\tau+1]}$, $\forall n$, we can derive $\widehat{\mathcal{Y}}_{\rm b}^{[\tau+1]}$ and $\widehat{\mathcal{Y}}_n^{[\tau+1]}, \forall n$, by solving the following problem:

$$\min_{\widehat{\mathcal{Y}}_{\rm b}, \{\widehat{\mathcal{Y}}_n\}_{n\in\mathcal{N}}} \mathcal{L}\left(\widehat{\mathcal{Y}}_{\rm b}, \boldsymbol{\psi}_{\rm b}^{[\tau+1]}, \left\{\widehat{\mathcal{Y}}_n, \boldsymbol{\psi}_n^{[\tau+1]}\right\}_{n\in\mathcal{N}}, \mathbf{\Lambda}^{[\tau]}\right) \quad (53)$$

s.t. $C14$.

Relaxing the binary variables $\widehat{y}_{k,\rm b}$'s and $\widehat{y}_{k,n}$'s to be real-valued variables taking values within $[0,1]$, we can also transform the problem given in Eq. (53) as a convex optimization problem, and then solve it easily. Since all SAPs are under the coverage of the BS b_0, the BS b_0 can perform the updating of $\widehat{y}_{k,\rm b}$'s and $\widehat{y}_{k,n}$'s by receiving $\boldsymbol{\psi}_n^{[\tau+1]}$ from each SAP n.

3) Updating Lagrange Multipliers in $\mathbf{\Lambda}$: Given the obtained $\widehat{\mathcal{Y}}_{\rm b}^{[\tau+1]}$ and $\widehat{\mathcal{Y}}_n^{[\tau+1]}, \forall n$, we can update $\mathbf{\Lambda} = \{\lambda_k, \mu_{k,n}, \forall k, n\}$ by using the following equations:

$$\begin{cases} \lambda_k^{[\tau+1]} = \lambda_k^{[\tau]} - \rho\left(\widehat{y}_{k,\rm b}^{[\tau+1]} - y_{k,\rm b}^{[\tau+1]}\right), & \forall k, \quad (54)\\ \mu_{k,n}^{[\tau+1]} = \mu_{k,n}^{[\tau]} - \rho\left(\widehat{y}_{k,n}^{[\tau+1]} - y_{k,n}^{[\tau+1]}\right), & \forall k, n. \quad (55)\end{cases}$$

Similar to the updating of $\widehat{y}_{k,\rm b}$'s and $\widehat{y}_{k,n}$'s, the BS b_0 can perform the Lagrange multipliers updating by receiving $\widehat{\mathcal{Y}}_n^{[\tau+1]}$ from each SAP n.

4) Algorithm Stopping Criterion and Convergence: Repeat the above three steps until the following stopping criterion

$$\sum_{k\in\mathcal{K}}\left(\left|\widehat{y}_{k,\rm b}^{[\tau]} - y_{k,\rm b}^{[\tau]}\right| + \sum_{n\in\mathcal{N}}\left|\widehat{y}_{k,n}^{[\tau]} - y_{k,n}^{[\tau]}\right|\right) \le \epsilon, \quad (56)$$

is satisfied, where ϵ is a very small value [34]. We summarize the proposed ADMM-based traffic-offloading and resource-allocation algorithm in **Algorithm 1**. As pointed out in [33], the ADMM-based **Algorithm 1** converges, since the dual problem given in Eq. (20) is a concave function with respect to $\mathbf{\Lambda}$. However, **Algorithm 1** may not converge to the primal-optimal solution of the problem given in Eq. (14), due to the potential duality gap between the non-convex optimization problem given in Eq. (14) and its dual problem given in Eq. (20). Therefore, the solution obtained by **Algorithm 1** may be an approximate solution to the problem given in Eq. (14).

Algorithm 1: ADMM-Based Distributed Traffic-Offloading and Resource-Allocation Schemes.

1. **Initialization**:
   a) Set the iteration index of the ADMM method as $\tau = 0$.
   b) The BS b_0 initializes $\widehat{\mathcal{Y}}_{\rm b}^{[0]}$ and $\widehat{\mathcal{Y}}_n^{[0]}$, $\forall n$, which satisfies C14.
   c) The BS b_0 initializes $\lambda_k^{[0]}$, $\forall k$. Each SAP n initializes $\mu_{k,n}^{[0]}$, $\forall k$, and sends them to the BS b_0.
   d) The BS b_0 determines the parameter ϵ in Eq. (56).
2. **Repeat**
   For given $\widehat{\mathcal{Y}}_{\rm b}^{[\tau]}$, $\widehat{\mathcal{Y}}_n^{[\tau]}$, $\forall n$, and $\mathbf{\Lambda}^{[\tau]} \triangleq \{\lambda_k^{[\tau]}, \mu_{k,n}^{[\tau]}, \forall k, n\}$, the BS b_0 solves the problem specified by Eq. (38) to obtain $\boldsymbol{\psi}_{\rm b}^{[\tau+1]} \triangleq \{\boldsymbol{\vartheta}_{\rm b}^{[\tau+1]}, \mathcal{P}_{\rm b}^{[\tau+1]}, \mathcal{S}_{\rm b}^{[\tau+1]}, \mathcal{Y}_{\rm b}^{[\tau+1]}\}$.
   Meanwhile, each SAP n solves the problem given in Eq. (51) to obtain
   $\boldsymbol{\psi}_n^{[\tau+1]} \triangleq \{\mathcal{Z}_n^{[\tau+1]}, \boldsymbol{\beta}_n^{[\tau+1]}, \mathcal{P}_n^{[\tau+1]}, \mathcal{Y}_n^{[\tau+1]}\}$, and then sends $\boldsymbol{\psi}_n^{[\tau+1]}$ to the BS b_0.
3. For given $\boldsymbol{\psi}_{\rm b}^{[\tau+1]}$, $\boldsymbol{\psi}_n^{[\tau+1]}$, $\forall n$, and $\mathbf{\Lambda}^{[\tau]}$, the BS b_0 solves the problem in Eq. (53) to obtain $\widehat{\mathcal{Y}}_{\rm b}^{[\tau+1]}$ and $\widehat{\mathcal{Y}}_n^{[\tau+1]}$, $\forall n$.
4. Based on the above-obtained $\widehat{\mathcal{Y}}_{\rm b}^{[\tau+1]}$ and $\widehat{\mathcal{Y}}_n^{[\tau+1]}$, $\forall n$, the BS b_0 updates the Lagrange multipliers $\lambda_k^{[\tau+1]}$ and $\mu_{k,n}^{[\tau+1]}$, $\forall n$, based on Eqs. (54)-(55), respectively.
5. Set $\tau = \tau + 1$.

Until The algorithm stopping criterion given in Eq. (56) is satisfied.

---

5) Binary Variables Recovery: Since we have relaxed the binary variables $y_{k,\rm b}$'s and $y_{k,n}$'s as real-valued variables, we need to recover the binary variables $y_{k,\rm b}$'s and $y_{k,n}$'s from the above-obtained solution. To minimize the energy consumption of all MUs, we recover the binary variables $y_{k,\rm b}$'s and $y_{k,n}$'s according to the following criterion:

$$y_{k,\rm b} = \begin{cases} 1, & \text{if } E_{k,\rm b} \le E_{k,n}, \forall n,\\ 0, & \text{otherwise,}\end{cases} \quad (57)$$

$$y_{k,n} = \begin{cases} 1, & \text{if } n = \operatorname*{argmin}_{l\in\mathcal{N}}\{E_{k,l}\} \text{ and } E_{k,n} \le E_{k,\rm b},\\ 0, & \text{otherwise.}\end{cases} \quad (58)$$

Based on the obtained binary variables $y_{k,\rm b}$'s and $y_{k,n}$'s, we can solve the original problem given in Eq. (14) easily to allocate resources for the cellular network and the WiFi network.

6) Algorithm Complexity: The complexity of the proposed algorithm mainly lies in solving the problems specified by Eqs. (38) and (51). For given $\mathcal{S}_{\rm b}$ and $\boldsymbol{\vartheta}_{\rm b}$, the problem specified by Eq. (38) is convex. Then, for given $\mathcal{S}_{\rm b}$ and $\boldsymbol{\vartheta}_{\rm b}$, the complexity of solving the problem given in Eq. (38) with $3K$ variables is $O((3K)^3)$ [39]. Similarly, for given $\mathcal{P}_{\rm b}$, $\mathcal{Y}_{\rm b}$, and $\widetilde{\mathcal{Y}}_{\rm b}$, the complexity of solving the problem given in Eq. (38) with $2K$ variables is $O((2K)^3)$. Moreover, each SAP n only needs to solve the problem specified by (51) for MUs under its coverage. The problem specified by (51) has at most $5K$ variables, and

Authorized licensed use limited to: Texas A M University. Downloaded on January 17,2022 at 20:42:04 UTC from IEEE Xplore. Restrictions apply.

then the complexity of solving this convex optimization problem is at most $O((5K)^3)$. Assuming that the maximum iteration number of the alternative optimization method using to solve the problem given in Eq. (38) is J_1, and the maximum iteration number of the ADMM method is J_2, then the total complexity of the Algorithm 1 is at most $O(J_1 J_2 (3K)^3 + N J_2 (5K)^3)$, where N is the number of the SAPs.

IV. Concurrent AB Aided Communication and Bistatic Scatter Aided Communication

A. Concurrent AB Aided Communication for WiFi Networks

For the AB communication, adopting the novel coding mechanism, i.e., μcode, proposed in [4], we can also consider the scenario when multiple MUs can backscatter signals concurrently without mutual interference, i.e., the concurrent ambient backscatter (CAB) mode, to further decrease the energy consumption. As pointed out in [4], μcode uses periodic alternating chip sequence of zeros and ones to represent information. Assuming that I MUs can backscatter data concurrently and they adopt the same chip length, to work in the CAB mode, the I MUs need to convey information with backscatter rates $B_0, 2B_0, \ldots,$ and $2(I-1)B_0$, respectively [4], where $B_0 > 0$ is a constant. For each SAP n, we group MUs accessing it into several clusters, and only MUs in the same cluster can backscatter signals concurrently. Then, based on the problem given in Eq. (14), we can formulate the optimization problem when the CAB mode is adopted as follows:

$$\min_{\boldsymbol{\psi}_{\mathrm{b}}, \{\boldsymbol{\psi}_n, \boldsymbol{\varsigma}_n, \boldsymbol{\delta}_n\}_{n\in\mathcal{N}}} \left(E_{\mathrm{b}} + \sum_{n\in\mathcal{N}} E_n\right) \tag{59}$$
$$\text{s.t. } C1, C3 - C11,$$
$$C15: \sum_{q\in\mathcal{Q}_n} \varsigma_{n,q} + \sum_{k\in\mathcal{K}} y_{k,n}\beta_{k,n} \le T, \forall n,$$
$$C16: \sum_{q\in\mathcal{Q}_n} y_{k,n}\delta_{k,n,q} \le 1, \forall k, n,$$
$$C17: \frac{y_{k,n}\delta_{k,n,q}(D_k - Z_{k,n})}{B_k} \le \varsigma_{n,q}, \forall k, n, q,$$
$$C18: \delta_{k,n,q} \le y_{k,n}, \forall k, n, q,$$

where $\mathcal{Q}_n$ is the set of clusters of SAP n, $\boldsymbol{\varsigma}_n \triangleq \{\varsigma_{n,q} \in [0,T], \forall q\}$, and $\boldsymbol{\delta}_n \triangleq \{\delta_{k,n,q} \in \{0,1\}, \forall k, q\}$, where $\varsigma_{n,q}$ is the backscatter time of MUs in cluster q of SAP n, and $\delta_{k,n,q}$, $\forall k, q$, is a binary variable, which is defined as:

$$\delta_{k,n,q} \triangleq \begin{cases} 1, \text{if MU } k \text{ belongs to cluster } q \text{ of SAP } n, \\ 0, \text{otherwise.} \end{cases} \tag{60}$$

$C15$ is the time consumption constraint of MUs when considering the CAB mode. $C16$ ensures that MU k can at most belong to one cluster. $C17$ states that the backscatter time of MU k cannot exceed $\varsigma_{n,q}$ if $\delta_{k,n,q} = 1$, and $C18$ ensures that only MUs accessing SAP n can be grouped into cluster q of SAP n.

Compared with the problem in Eq. (14), the problem given in Eq. (59) is more difficult to solve, since we also need to determine which cluster each MU k should belong to. Hence, we will propose a suboptimal algorithm. First, we solve the problem in Eq. (14), where for the AB mode, we assume that the backscatter rate B_k of MU k, $\forall k \in \mathcal{K}$, is the maximum achievable backscatter rate $B^{\max}$ for a specific transceiver design. After solving the problem in Eq. (14), we assume that $\mathcal{G}_n \triangleq \{k | y_{k,n} = 1, \forall k \in \mathcal{K}\}$ is the set of MUs accessing SAP n. Then, based on the solution to the problem in Eq. (14), we determine which cluster MU k, $\forall k \in \mathcal{G}_n$, should belong to when employing the CAB mode by using **Algorithm 2**.[6]

In **Algorithm 2**, the aim of Step 1 is to guarantee that each MU's throughput through concurrent backscatter is not less than that without concurrent backscatter. For example, if $\alpha_{k,n} = 0.1$ s and $\alpha_{k',n} = 0.05$ s, we can group MUs k and k' into the same cluster q, and set $\varsigma_{n,q} = \alpha_{k,n} + \alpha_{k',n}$, $B_k = B^{\max}$, and $B_{k'} = 0.5B^{\max}$ in the CAB mode. Then, compared with the AB mode, the throughputs of both MUs k and k' will not decrease through the CAB mode. In addition, we can adopt the similar method as that in Step 2 to group MU k with $y_{k,\mathrm{b}} = 1$ into a suitable cluster in $\mathcal{Q}_n$, if there exists a cluster q such that $E^{\mathrm{s}}_{k,n,q} > 0$, and the distance between MU k and SAP n is not larger than $d_{\max}$, which is the maximum distance to establish the AB communication for a specific transceiver design. Then, we can update the set $\mathcal{G}_n$ and obtain the set $\boldsymbol{\delta}_n \triangleq \{\delta_{k,n,q} \in \{0,1\}, \forall k, q\}$, where $\delta_{k,n,q}$ is defined in Eq. (60).

Based on the obtained $\boldsymbol{\delta}_n$, we solve the following convex optimization problem to determine resource-allocation for SAP n.

$$\min_{\mathcal{P}_n, \boldsymbol{\varsigma}_n, \mathcal{Z}_n, \boldsymbol{\beta}_n} \sum_{k\in\mathcal{G}_n} E_{k,n} \tag{61}$$
$$\text{s.t. } C19: \sum_{q\in\mathcal{Q}_n} \varsigma_{n,q} + \sum_{k\in\mathcal{G}_n} \beta_{k,n} \le T,$$
$$C20: E_{k,n} + P_{\mathrm{c}}\beta_{k,n} \le \left\{E^{\mathrm{h}}_{k,n}, E^{\max}_k\right\}, \forall k \in \mathcal{G}_n,$$
$$C21: P_{k,n} \le P^{\max}_k, \forall k \in \mathcal{G}_n,$$
$$C22: \frac{\delta_{k,n,q}(D_k - Z_{k,n})}{B_k} \le \varsigma_{n,q}, \forall k \in \mathcal{G}_n,$$

where for MU k, $k \in \mathcal{G}(n)$, $C19$ and $C22$ are the time consumption constraints, and $C20$-$C21$ are the energy consumption and power consumption constraints, respectively.

B. Bistatic Scatter Aided Communication for Cellular Networks

We can also employ the long-range bistatic backscatter (BB) technique to further decrease the energy consumption of MUs accessing the BS b_0. Different from the AB communication, the BB communication has a long communication range (up to about 270 meters) [10]. Adopting the BB technique, MU k can backscatter information to the BS b_0, i.e., working in the BB mode, by modulating their information bits to the unmodulated

[6] Since the solution to the CAB case is based on the solution to the non-concurrent backscatter case, for ease of presentation, we consider the two cases separately. Moreover, since we need to determine which cluster each MU belongs to in the CAB case, the implementation complexity of the CAB is relatively higher than that of the non-concurrent backscatter. Hence, by considering the two cases separately, MUs can select suitable backscatter modes based on their requirements.

Authorized licensed use limited to: Texas A M University. Downloaded on January 17,2022 at 20:42:04 UTC from IEEE Xplore. Restrictions apply.

Algorithm 2: The Clustering Algorithm for Concurrent Ambient Backscatter.

1. **Step 1:**
Input: Load the sets of $\mathcal{Y}_{\rm b} \triangleq \{y_{k,{\rm b}}, \forall k\}$ and $\mathcal{Y}_n \triangleq \{y_{k,n}, \forall k\}, \forall n$, and the backscatter time $\alpha_{k,n}$'s obtained by solving the problem given in Eq. (14). Denote $\mathcal{G}_n \triangleq \{k | y_{k,n} = 1, \forall k \in \mathcal{K}\}$ as the set of MUs which choose to access SAP n.
2. **Step 2:**
2.1. For $\forall k,\, k' \in \mathcal{G}_n$, calculate $\alpha_{k,n}/\alpha_{k',n}$. Besides, define a $K \times K$ matrix $\mathbf{\Upsilon} \triangleq [\upsilon(k,k')]$, where for MUs $k, k' \in \mathcal{K}$, if $k, k' \in \mathcal{G}_n$, then $\upsilon(k,k') \triangleq \alpha_{k,n}/\alpha_{k',n}$; otherwise $\upsilon(k,k') \triangleq 0$.
2.2. Define a $K \times K$ matrix $\mathbf{C} \triangleq [C(k,k')]$, where we first let $C(k,k') = 0$ for $\forall k, k' \in \mathcal{K}$. Then, for $k \in \mathcal{G}_n$, if k' is the only MU with $\upsilon(k,k') \geq 2$, and $\sum_{\iota \in \mathcal{K}} C(\iota, k') = 0$, we group MUs k and k' into the same cluster, and define $C(k,k') = 1$. If there exist more than one MU, e.g., two MUs k' and k'', satisfying $\upsilon(k,k') \geq \upsilon(k,k'') \geq 2$, and $\sum_{\iota \in \mathcal{K}} C(\iota, k') = \sum_{\iota \in \mathcal{K}} C(\iota, k'') = 0$, then we group MUs k and k'' into the same cluster, and let $C(k,k'') = 1$.
2.3. If MUs k and k' are grouped into cluster q of SAP $n \in \mathcal{N}$, and MUs k and k'' are grouped into q' of SAP n, then we group MUs k, k', and k'' into the same cluster. For SAP n, denote the set of clusters containing at least two MUs as $\mathcal{C}_n$.
3. **Step 3:**
3.1. If MU k, $k \in \mathcal{G}_n$, does not belong to any cluster of $\mathcal{C}_n$, we determine which cluster of $\mathcal{C}_n$ it should belong to. For cluster q, $\forall q \in \mathcal{C}_n$, assuming $\delta_{k,n,q} = 1$, we set the backscatter time of cluster q as $\varsigma_{n,q} = \sum_{\iota, \delta_{\iota,n,q}=1} \alpha_{\iota,n}$.
3.2. Sorting MUs in cluster q in descending order of $\alpha_{\iota,n}$'s, we set $B_\iota = B^{\max}\ \ 2^{(\nu-1)}$ for each MU ι in cluster q, where ν is the position of MU ι in the above-sorted sequence.
3.3. For each MU ι in cluster q of SAP n, we calculate $Z_{\iota,n}$ using $\varsigma_{n,q} = (D_\iota - Z_{\iota,n})/B_\iota$. If $Z_{\iota,n} = 0$, then energy consumption $E_{\iota,n} = 0$. If $Z_{\iota,n} \neq 0$, then we estimate energy $E_{\iota,n}$ by using $E_{\iota,n} = P_\iota^{\max} Z_{\iota,n}/R_{\iota,n}^{\max}$, where $R_{\iota,n}^{\max}$ is calculated by using $R_{\iota,n}^{\max} = W_n \log_2(1 + P_\iota^{\max} |h_{\iota,n}|^2\ /N_0\,)$.
3.4. Estimate the total energy saving $E_{k,n,q}^{\rm s}$ of all MUs in cluster q by comparing the energy consumption with and without the use of the CAB mode. For MU k, assuming that cluster q^* is the cluster leading to the largest energy saving, and $E_{k,n,q^*}^{\rm s} \geq 0$, then we group MU k into cluster q^*, $q^* \in \mathcal{C}_n$.
4. **Step 4:**
4.1. For $k \in \mathcal{G}_n$ which does not belong to any cluster in q, $\forall q \in \mathcal{C}_n$, we utilize the similar method as that in Step 2 to group these MUs into new clusters.
4.2. Denote all clusters obtained by the above three steps as $\mathcal{Q}_n$.

carrier signals emitted from some carrier emitters (CEs). We assume that there exist M CEs, denoted by $\mathcal{M} \triangleq \{1, 2, \ldots, M\}$, in our network system depicted in Fig. 1, and then each MU can switch between the HTT mode and the BB mode when communicating with the BS b_0. As shown in Fig. 4, for all MUs accessing the BS b_0, we denote $\theta_{\rm b}$ and $\chi_{\rm b}$ as the common time periods for energy harvesting and data transmission in the HTT mode, respectively, where similar to Section II-B, MUs transmit data to the BS b_0 during the time period $\chi_{\rm b}$ using orthogonal spectrums in the HTT mode. Besides, for MU k, we denote $\rho_{k,{\rm b}}$ as the time period for the BB mode. Assuming that $\phi_{k,{\rm b}}$ bits of MU k's data are to be transmitted through the HTT mode, then similar to Eq. (9), we can express the energy consumption of MU k when accessing the BS b_0 as:

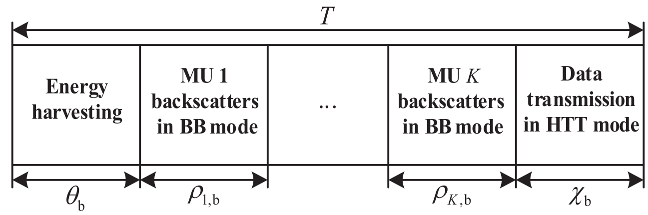

Fig. 4. The cooperation between MUs and the BS b_0 aided by the bistatic backscatter (BB) communication.

$$E_{k,{\rm b}} = \frac{\chi_{\rm b}}{|h_{k,{\rm b}}|^2} f\left(\frac{\phi_{k,{\rm b}}}{\chi_{\rm b} s_{k,{\rm b}} W_{\rm b}}\right), \tag{62}$$

where similar to Section II-B, if $\chi_{\rm b} = 0$ or/and $s_{k,{\rm b}} = 0$, we can define $E_{k,{\rm b}} = 0$ when $\phi_{k,{\rm b}} = 0$. If $\chi_{\rm b} = 0$ or/and $s_{k,{\rm b}} = 0$ while $\phi_{k,{\rm b}} > 0$, we can define $E_{k,{\rm b}}$ as a value which is larger than the maximum capacity $E_k^{\max}$ of MU k's energy storage.

We assume that the CEs can work in the same spectrum with the BS, but they work in different spectrums with the ES and the SAPs. Hence, for the considered communication scenarios, similar to the problem in Eq. (14), we can formulate the traffic-offloading and resource-allocation problem as follows:

$$\min_{\boldsymbol{\varphi}_{\rm b}, \{\boldsymbol{\psi}_n\}_{n\in\mathcal{N}}} \left(E_{\rm b} + \sum_{k\in\mathcal{K}} P_{{\rm ce,b}} y_{k,{\rm b}} \rho_{k,{\rm b}} + \sum_{n\in\mathcal{N}} E_n\right) \tag{63}$$

s.t. $C2, C4 - C9,$

$$C23: \theta_{\rm b} + \sum_{k\in\mathcal{K}} y_{k,{\rm b}}\rho_{k,{\rm b}} + \chi_{\rm b} \leq T,$$

$$C24: y_{k,{\rm b}}\left(E_{k,{\rm b}} + P_{\rm c}\chi_{\rm b} + P_{{\rm ce,b}}\rho_{k,{\rm b}}\right) \leq \min\left\{E_{k,{\rm b}}^{\rm h}, E_k^{\max}\right\}, \forall k,$$

$$C25:\ \mathbb{1}\left(P_{\rm e}|h_{{\rm e},k}|^2 + \sum_{m\in\mathcal{M}} P_m |h_{m,k}|^2 < d_k\right)\rho_{k,{\rm b}} \geq 0, \forall k,$$

$$C26:\ \mathbb{1}\left(P_{\rm e}|h_{{\rm e},k}|^2 + \sum_{m\in\mathcal{M}} P_m |h_{m,k}|^2 < d_k\right)\phi_{k,{\rm b}} = 0, \forall k,$$

$$C27:\ \mathbb{1}\left(P_{\rm e}|h_{{\rm e},k}|^2 + \sum_{m\in\mathcal{M}} P_m |h_{m,k}|^2 < d_k\right)\beta_{k,n} = 0, \forall k, n,$$

where $\boldsymbol{\rho}_{\rm b} \triangleq \{\rho_{k,{\rm b}}, \forall k\}$, $\boldsymbol{\varphi}_{\rm b} \triangleq \{\theta_{\rm b}, \chi_{\rm b}, \boldsymbol{\rho}_{\rm b}, \mathcal{Y}_{\rm b}, \mathcal{S}_{\rm b}, \mathcal{P}_{\rm b}\}$, and $E_{\rm b}$ and E_n are defined in Eqs. (15)-(16), respectively, P_m is the transmit power of CE m, $\forall m \in \mathcal{M}$, $h_{m,k}$ is the channel power gain from CE m to MU k, and $P_{{\rm ce,b}}$ is the power consumption of MU k when backscattering data to the BS b_0 in the BB mode. Besides, $C23$-$C24$ are the time consumption and energy consumption constraints of MU k, respectively, when accessing the BS b_0. $C25$-$C27$ are similar to $C10$-$C11$, which state that

Authorized licensed use limited to: Texas A M University. Downloaded on January 17,2022 at 20:42:04 UTC from IEEE Xplore. Restrictions apply.

if the received power level, i.e., $P_{\rm e}|h_{{\rm e},k}|^2 + \sum_{m\in\mathcal{M}} P_m|h_{m,k}|^2$, at MU k is less than d_k, then MU k can only work in the BB or AB mode. Moreover, similar to [8], [17], we assume that MUs can use the dual-band antenna to harvest energy from RF signals emitted from both the ES and the CEs.[7] Therefore, for the considered communication scenarios, similar to Eq. (13), we can write the harvested energy at MU k when accessing the BS b_0 and SAP n, respectively, as follows:

$$\begin{cases} E^{\rm h}_{k,{\rm b}} = \left[\frac{\Phi_k\left(P_{\rm e}|h_{{\rm e},k}|^2+\sum_{m\in\mathcal{M}} P_m|h_{m,k}|^2\right)-M_k\Omega_k}{1-\Omega_k}\right] \\ \qquad \times\left(\sum_{k'\neq k}\frac{D_{k'}-\phi_{k',{\rm b}}}{B^{\rm bs}_{k'}}+\theta_{\rm b}\right), & (64) \\ E^{\rm h}_{k,n} = \left[\frac{\Phi_k\left(P_{\rm e}|h_{{\rm e},k}|^2+\sum_{m\in\mathcal{M}} P_m|h_{m,k}|^2\right)-M_k\Omega_k}{1-\Omega_k}\right] \\ \qquad \times\left(\sum_{k'\neq k}\frac{D_{k'}-Z_{k',n}}{B_{k'}}+\beta_{k,n}\right), & (65) \end{cases}$$

where $B^{\rm bs}_{k'}$ is the backscatter rate of MU k' in the BB mode. Similar to [8], [17], we assume that when the BB mode is activated, the binary frequency-shift keying (FSK) modulation is performed at MU k', then we can express $B^{\rm bs}_{k'}$ as follows:

$$B^{\rm bs}_{k'} = W_{\rm ce}\log_2\left(1+\frac{P_{{\rm ce},k',{\rm b}}|h_{k',{\rm b}}|^2}{\zeta^{\rm bs}_{k'}N_0}\right), \quad (66)$$

where similar to ζ_k in Eq. (2), $\zeta^{\rm bs}_{k'}$ is introduced to measure the performance gap between the backscatter rate $B^{\rm bs}_{k'}$ and the channel capacity from MU k' to the BS b_0 [26]–[28]. In addition, since MU k has already spent a time period of $\theta_{\rm b}$ for energy harvesting, we assume that MU k uses the received signal from CE m only for data backscattering in Eq. (66) to support a long communication range of the BB mode, instead of splitting it for data backscattering and energy harvesting as in [13]. $W_{\rm ce}$ is the bandwidth of the CEs, and $P_{{\rm ce},k',{\rm b}}$ is the transmit power from MU k' to the BS b_0 in the BB mode, which can be expressed as:

$$P_{{\rm ce},k',{\rm b}} = \sum_{m\in\mathcal{M}} P_m|h_{m,k'}|^2\xi^2_{k'}\left(\frac{\Gamma_0-\Gamma_1}{2}\right)^2\left(\frac{4}{\pi}\right)^2, \quad (67)$$

where for MU k', $\xi_{k'}$ is the scattering efficiency, and Γ_0 and Γ_1 are the reflection coefficients specified by the load impedances [8]. Similar to the problem given in Eq. (14), we can decompose the problem specified by Eq. (63) into several subproblems using ADMM, and solve each subproblem using the RLT, the alternative optimization, and so on.

V. Performance Evaluations

We consider a circular area, where the BS is located at the origin, while all SAPs and MUs are randomly distributed in the area. Similar to [40], we assume that $h_{k,{\rm b}} \triangleq h'_{k,{\rm b}}d^{\gamma_{k,{\rm b}}}_{k,{\rm b}}$, $h_{k,n} \triangleq h'_{k,n}d^{\gamma_{k,n}}_{k,n}$, $h_{{\rm e},k} \triangleq h'_{{\rm e},k}d^{\gamma_{{\rm e},k}}_{{\rm e},k}$, and $h_{m,k} \triangleq h'_{m,k}d^{\gamma_{m,k}}_{m,k}$,

[7]Dual-band energy harvesting techniques can be utilized by low-power MUs, as shown in [17] and references therein. Since the transmit power of each CE is generally very low, MU k may only be able to harvest energy from CEs deployed nearby. Similarly, in the BB mode, MU k may only be able to convey data by reflection of unmodulated signals radiated from CEs deployed nearby.

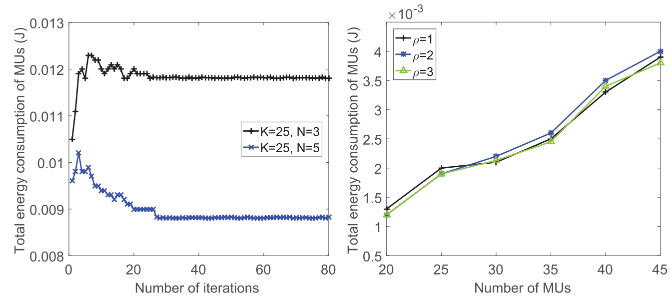

(a) (b)

Fig. 5. Convergence performance of the ADMM-based traffic-offloading and resource-allocation schemes. (a) Convergence of our proposed scheme when the AB mode is used to accommodate data transmission. (b) Total energy consumption of MUs with the assistance of the CAB mode.

where $h'_{k,{\rm b}}$, $h'_{k,n}$, $h'_{{\rm e},k}$, and $h'_{m,k}$ denote the corresponding small-scale fadings, $d_{k,{\rm b}}$ and $d_{k,n}$ are the distances from MU k to the BS b_0 and SAP n, respectively, $d_{{\rm e},k}$ and $d_{m,k}$ are the distances from the ES and CE m to MU k, respectively, and $\gamma_{k,{\rm b}}$, $\gamma_{k,n}$, $\gamma_{{\rm e},k}$, and $\gamma_{m,k}$ are the path loss exponents of the large-scale fadings. We assume that $h'_{k,{\rm b}}$ follows Rayleigh fading, while $h'_{k,n}$, $h'_{m,k}$, and $h'_{{\rm e},k}$ follow Rician fading, since Rician fading is more appropriate to take into account the effect of line-of-sight component in RF-based EH systems [41]. For large-scale fadings, we take $\gamma_{k,{\rm b}} = 3$ and $\gamma_{k,n} = \gamma_{{\rm e},k} = \gamma_{m,k} = 2.5$. We consider the following two network scenarios. In **Scenario I**, we set the radius of the considered circular area as $r = 55$ m. For the AB communication, we take the maximum achievable backscatter rate $B^{\max} = 1$ Kbps and the maximum communication range $d^{\max} = 24$ m realized by the prototype in [4]. Since $B^{\max} = 1$ Kbps, we assume that the input data sizes of MUs follow uniform distribution with $D_k \in [3\times10^2, 6\times10^2]$ bits. For **Scenario II**, we set $r = 10$ m, and take $B^{\max} = 1$ Mbps and $d^{\max} = 5$ m realized by the AB prototype in [7]. Since $B^{\max}$ takes a relatively large value, i.e., 1 Mbps, we set $D_k \in [3\times10^4, 6\times10^4]$ bits. Unless otherwise specified, we let $K = 25$ and $N = 5$, since there generally exist a large number of MUs and/or SAPs in today's wireless networks. We take $P_m = 0.02$ W and $M = 5$, since the CE generally transmits at a low power level and needs to be deployed near the MUs [17]. In addition, we take $P_{\rm e} = 3$ W, $P_{\rm c} = 10^{-4}$ W, $T = 1$ s, $\rho = 2$, $W_{\rm b} = 4$ MHz, and $W_n = 1$ MHz. Furthermore, for the BB mode, we take $\Gamma_0 = 1$ and $\Gamma_1 = -1$, and set the scattering efficiency $\xi_k = 0.7$ [8].

For **Scenario I**, Fig. 5(a) shows that our proposed schemes yield the satisfactory convergence performance, which enables our proposed schemes to converge to the targeted optimal solution within around 25 iterations. Besides, Fig. 5(b) shows the total energy consumption of MUs versus the penalty parameter ρ, which can control the convergence speed of ADMM. We can see that the total energy consumption of MUs obtained for different ρ converges to almost the same value for given number of MUs, i.e., K. Moreover, Fig. 5(b) also shows that when the CAB mode is utilized, the total energy consumption of MUs can be significantly reduced, especially when K is large. This is because by grouping MUs into different clusters using

Authorized licensed use limited to: Texas A M University. Downloaded on January 17,2022 at 20:42:04 UTC from IEEE Xplore. Restrictions apply.

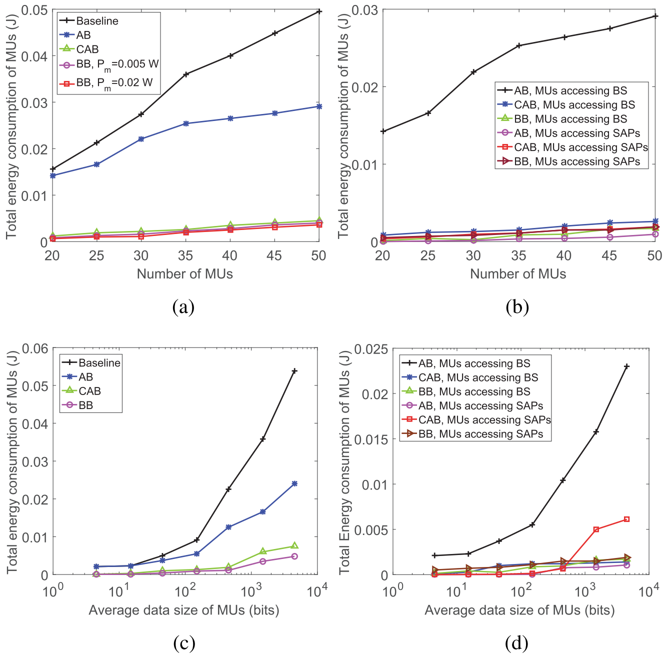

Fig. 6. Total energy consumption of MUs versus the number of MUs, i.e., K, and the average data size of MUs, i.e., $\sum_{k\in\mathcal{K}} D_k/K$. (a) Total energy consumption of MUs versus K; (b) Total energy consumption of MUs accessing the BS or the SAPs versus K; (c) Total energy consumption of MUs versus $\sum_{k\in\mathcal{K}} D_k/K$; (d) Total energy consumption of MUs accessing the BS or the SAPs versus $\sum_{k\in\mathcal{K}} D_k/K$.

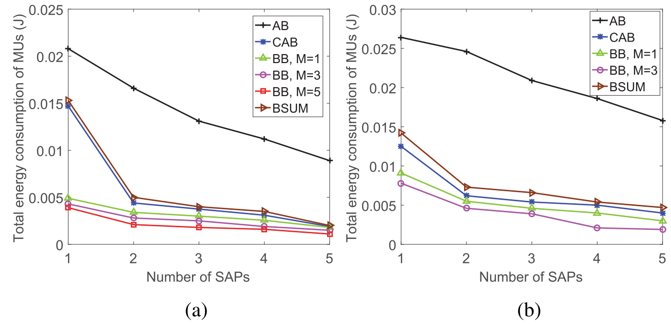

Fig. 7. Total energy consumption of MUs versus the number of SAPs, i.e., N. (a) Total energy consumption of MUs versus N for network **Scenario I**; (b) Total energy consumption of MUs versus N for network **Scenario II**.

Algorithm 2 and adopting the CAB mode, MUs belonging to the same cluster can backscatter data concurrently with longer backscatter time. Furthermore, as K increases, more MUs, e.g., MUs previously accessing the BS b_0, can be grouped into suitable clusters, and backscatter data to suitable SAPs.

Fig. 6 shows the energy consumption of MUs versus the number of MUs, i.e., K, and the average data size of MUs, i.e., $\sum_{k\in\mathcal{K}} D_k/K$, for **Scenario I**. For comparison, we also show the numerical results obtained by a baseline algorithm, where all MUs can only access the BS b_0 and work in the HTT mode. Figs. 6(a) and (c) show that due to the assistance of backscatter, the total energy consumption of MUs can be reduced and the performance gain over the baseline algorithm increases as $\sum_{k\in\mathcal{K}} D_k/K$ or K increases. This is because when MUs work in the HTT mode, they need to actively transmit information. Hence, the energy consumption of MUs is much higher when only working in the HTT mode, compared with the scenarios when working with the assistance of backscatter. This can also be seen from Figs. 6(b) and (d), where the energy consumption of MUs accessing the BS b_0 is generally much higher than that of MUs accessing the SAPs. Furthermore, Figs. 6(a) and (c) also show that when the BB communication is used to assist the data transmission of MUs accessing the BS, the total energy consumption of MUs can be further reduced, and the energy consumption of MUs accessing the BS is comparable to that of MUs accessing the SAPs. The above results also confirm the low-energy consumption of the backscatter communications. In addition, the total energy consumption of MUs increases significantly as K increases or as $\sum_{k\in\mathcal{K}} D_k/K$ increases from 1.5×10^2 bits to 4.5×10^3 bits, especially when the baseline algorithm or the AB mode is used to assist data transmission. Also, the total energy consumption of MUs can be slightly reduced as P_m changes from 0.005 W to 0.02 W.

Fig. 7 shows the total energy consumption of MUs versus the number of SAPs, i.e., N, for **Scenarios I-II**. Notice that since some MUs, e.g., security microphones/cameras recording audio/video, produce throughputs in the order of a few Mbps, the wireless links from these MUs to the wired gateway connected to the Internet should provide at least a few Mbps of uplink transmissions at a range of 1-5 meters [7]. Thus, we consider **Scenario II** which has a maximum backscatter rate in the order of 1 Mbps at a range of 5 meters in Fig. 7(b). For **Scenarios I-II**, Fig. 7 shows that the total energy consumption of MUs decreases significantly with the increase of N, when the AB mode or the CAB mode is used. This is because when N increases, more and more MUs can choose to access suitable SAPs and backscatter data to these SAPs with negligible energy consumption. However, when the BB mode is also used, a relatively small performance gain can be obtained with the increase of N. This is because compared with the CAB mode, when the BB communication is leveraged, extra system performance gain is mainly due to the decrease of energy consumption of MUs accessing the BS and working in the BB mode. Moreover, the total energy consumption of MUs decreases as the number of CEs, i.e., M, increases, since more and more MUs can work in the BB mode when M increases. In addition, Fig. 7 shows that the energy consumption of MUs obtained by the schemes based on the widely adopted BSUM method [35] is slightly higher than that obtained by our ADMM-based schemes, where the CAB mode is utilized.

Fig. 8 depicts the energy consumption of MUs versus the bandwidth of the BS b_0, i.e., W_{b}, and the maximum backscatter rate of MUs, i.e., $B^{\max}$, for **Scenarios I-II**. Since we take $W_n = 1$ MHz for SAP n similar to [8], in Fig. 8(a), we take W_{b} from 2 MHz to 14 MHz for the BS, which generally has a higher bandwidth than SAP n, to evaluate the effect of W_{b} on system performance. Fig. 8 shows that the energy consumption of MUs decreases significantly with the increase of W_{b} or $B^{\max}$, when the CAB mode with $N = 1$ or the AB mode is utilized. However,

Authorized licensed use limited to: Texas A M University. Downloaded on January 17,2022 at 20:42:04 UTC from IEEE Xplore. Restrictions apply.

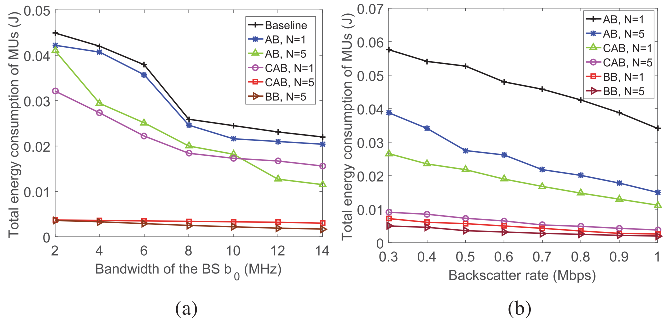

Fig. 8. Total energy consumption of MUs versus the bandwidth of the BS, i.e., W_{b}, and MUs' backscatter rate, i.e., B_k. (a) Total energy consumption of MUs versus W_{b} for network **Scenario I**; (b) Total energy consumption of MUs versus B_k for network **Scenario II**.

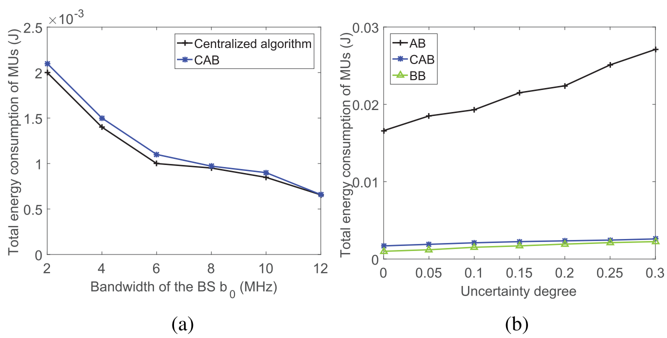

Fig. 9. Performance comparison with the centralized algorithm and total energy consumption of MUs versus different levels of uncertainty degree. (a) Performance comparison with the centralized algorithm; (b) Total energy consumption of MUs versus different levels of uncertainty degree.

small performance gains can be obtained with the increase of W_{b} when the CAB mode (with $N = 5$) or the BB mode is used. The above results are all because of the low-energy consumption of the backscatter communications.

Fig. 9(a) shows the performance comparison of our proposed schemes with the centralized algorithm, where different MUs can backscatter data concurrently. We take $K = 10$ and $N = 2$. Fig. 9(a) shows that when the CAB mode is utilized, system performance obtained by our ADMM-based schemes is very close to that of the centralized algorithm. Moreover, Fig. 9(b) shows the energy consumption of MUs when the system CSI cannot be perfectly estimated. Similar to [42], since the large-scale fadings vary slowly, we assume that the large-scale fadings can be perfectly estimated. For small-scale fadings, we assume that the channel estimation errors vary linearly with the estimated small-scale fadings. To this end, for the channel gain $h_{k,\mathrm{b}}$ defined in Eq. (2), we let $\widehat{h}'_{k,\mathrm{b}}$ (where $h'_{k,\mathrm{b}}$ is defined in the first paragraph of Section V) denote the estimated small-scale fading from MU k to the BS b_0, and also denote $\Delta h'_{k,\mathrm{b}}$ as the corresponding channel estimation error, where $|\Delta h'_{k,\mathrm{b}}|^2 \triangleq \varrho|\widehat{h}'_{k,\mathrm{b}}|^2$ with ϱ denoting the channel uncertainty degree due to the CSI estimation inaccuracy. Fig. 9(b) shows that although the energy consumption of MUs increases as ϱ increases, which may degrade the transmission rates and backscatter rates of MUs as indicated in Fig. 8(b), the impact of CSI's inaccuracy on the energy-consumption performance and transmission-rates performances for our proposed schemes is virtually neglectable for scheme CAB and scheme BB, but slightly higher for scheme AB, verifying the average robustness of our proposed schemes.

VI. Conclusions

We focused on the joint traffic-offloading and resource-allocation for RF-powered backscatter wireless networks, where a cellular BS, several SAPs, and multiple EH MUs coexist. Our aim is to minimize MUs' energy consumption by using the backscatter communications. First, we proposed a distributed traffic-offloading and resource-allocation scheme, when the AB communication is employed by MUs accessing the SAPs. Then, we considered the traffic-offloading and resource-allocation when MUs accessing the SAPs can work in the CAB mode. Moreover, we also studied the joint traffic-offloading and resource-allocation when the AB and BB communications are adopted by MUs accessing the SAPs and the BS, respectively. Finally, we validated and evaluated the performance of our proposed schemes through numerical analyses.

Appendix A

Using Eqs. (2)-(3), we can rewrite $T_{k,\mathrm{b}}$ for MU k accessing the BS b_0 as follows:

$$T_{k,\mathrm{b}} = D_k \left[s_{k,\mathrm{b}} W_{\mathrm{b}} \log_2 \left(1 + \frac{P_{k,\mathrm{b}} |h_{k,\mathrm{b}}|^2}{N_0} \right) \right]^{-1}. \quad (68)$$

Using Eq. (3) and $T_{k,\mathrm{b}} = (1 - \vartheta_{k,\mathrm{b}}) T$ given in Eq. (26), we can obtain that

$$\frac{1}{(1-\vartheta_{k,\mathrm{b}})\, T} = \frac{1}{D_k} \left[s_{k,\mathrm{b}} W_{\mathrm{b}} \log_2 \left(1 + \frac{P_{k,\mathrm{b}} |h_{k,\mathrm{b}}|^2}{N_0} \right) \right]. \quad (69)$$

Then,

$$\frac{y_{k,\mathrm{b}}}{(1-\vartheta_{k,\mathrm{b}})\, T} = \frac{y_{k,\mathrm{b}}}{D_k} \left[s_{k,\mathrm{b}} W_{\mathrm{b}} \log_2 \left(1 + \frac{P_{k,\mathrm{b}} |h_{k,\mathrm{b}}|^2}{N_0} \right) \right]. \quad (70)$$

Since $y_{k,\mathrm{b}} \in \{0, 1\}$, using Eq. (70), it is easy to get that

$$\frac{y_{k,\mathrm{b}}}{(1-\vartheta_{k,\mathrm{b}})\, T} = \frac{1}{D_k} \left[s_{k,\mathrm{b}} W_{\mathrm{b}} \log_2 \left(1 + \frac{y_{k,\mathrm{b}} P_{k,\mathrm{b}} |h_{k,\mathrm{b}}|^2}{N_0} \right) \right]. \quad (71)$$

For ease of mathematical tractability, we rewrite Eq. (71) as Eq. (29), i.e.,

$$\frac{y_{k,\mathrm{b}}}{(1-\vartheta_{k,\mathrm{b}})\, T} \leq \frac{1}{D_k} \left[s_{k,\mathrm{b}} W_{\mathrm{b}} \log_2 \left(1 + \frac{y_{k,\mathrm{b}} P_{k,\mathrm{b}} |h_{k,\mathrm{b}}|^2}{N_0} \right) \right],$$

where the equality holds when the optimization problem specified by Eq. (22) attains the optimal solution.

Authorized licensed use limited to: Texas A M University. Downloaded on January 17,2022 at 20:42:04 UTC from IEEE Xplore. Restrictions apply.

APPENDIX B
PROOF OF THEOREM 1

Proof: Since $y_{k,\mathrm{b}} \in \{0,1\}$ and $0 \leq P_{k,\mathrm{b}} \leq P_k^{\max}$, using the RLT, we can obtain the following inequalities:

$$\begin{cases} (y_{k,\mathrm{b}}-0)(P_{k,\mathrm{b}}-0) \geq 0, & (72)\\ (y_{k,\mathrm{b}}-1)(P_{k,\mathrm{b}}-0) \leq 0, & (73)\\ (y_{k,\mathrm{b}}-1)(P_{k,\mathrm{b}}-P_k^{\max}) \geq 0, & (74)\\ (y_{k,\mathrm{b}}-0)(P_{k,\mathrm{b}}-P_k^{\max}) \leq 0, & (75)\end{cases}$$

Plugging $\widetilde{P}_{k,\mathrm{b}}$ defined in Eq. (31) into Eqs. (72)-(75), we can obtain Eqs. (32)-(34).

Then, we prove that if the variable $\widetilde{P}_{k,\mathrm{b}}$ satisfies Eqs. (32)-(34), the equation $\widetilde{P}_{k,\mathrm{b}} = y_{k,\mathrm{b}}P_{k,\mathrm{b}}$ must hold. When the binary variable $y_{k,\mathrm{b}} = 0$, we can obtain that $\widetilde{P}_{k,\mathrm{b}} = 0$ from Eqs. (32) and (34). Hence, $\widetilde{P}_{k,\mathrm{b}}$ can be written as:

$$\widetilde{P}_{k,\mathrm{b}} = g(y_{k,\mathrm{b}}, P_{k,\mathrm{b}})y_{k,\mathrm{b}}, \tag{76}$$

where $g(\cdot)$ is a function with respect to $y_{k,\mathrm{b}}$ and $P_{k,\mathrm{b}}$. Now, using Eqs. (33)-(34) and Eq. (76), we can obtain that when $y_{k,\mathrm{b}} = 1$, the following equation holds.

$$g(1, P_{k,\mathrm{b}}) = P_{k,\mathrm{b}}. \tag{77}$$

Therefore,

$$g(y_{k,\mathrm{b}}, P_{k,\mathrm{b}}) = P_{k,\mathrm{b}}y_{k,\mathrm{b}}^{\omega}, \tag{78}$$

where $\omega \geq 0$. Plugging Eq. (78) into Eq. (76), we can obtain

$$\widetilde{P}_{k,\mathrm{b}} = P_{k,\mathrm{b}}y_{k,\mathrm{b}}^{\omega+1}. \tag{79}$$

Since $y_{k,\mathrm{b}} \in \{0,1\}$, we can directly write Eq. (79) as $\widetilde{P}_{k,\mathrm{b}} = y_{k,\mathrm{b}}P_{k,\mathrm{b}}$. ■

REFERENCES

[1] D. T. Hoang, D. Niyato, P. Wang, D. I. Kim, and Z. Han, "Ambient backscatter: A new approach to improve network performance for RF-powered cognitive radio networks," *IEEE Trans. Commun.*, vol. 65, no. 9, pp. 3659–3674, Sep. 2017.

[2] B. Clerckx, Z. B. Zawawi, and K. B. Huang, "Wirelessly powered backscatter communications: Waveform design and SNR-energy tradeoff," *IEEE Commun. Lett.*, vol. 21, no. 10, pp. 2234–2237, Oct. 2017.

[3] V. Liu, A. Parks, V. Talla, S. Gollakota, D. Wetherall, and J. R. Smith, "Ambient backscatter: Wireless communication out of thin air," *ACM SIGCOMM Comput. Commun. Rev.*, vol. 43, no. 4, pp. 39–50, Aug. 2013.

[4] A. N. Parks, A. Liu, S. Gollakota, and J. S. Smith, "Turbocharging ambient backscatter communication," *ACM SIGCOMM Comput. Commun. Rev.*, vol. 44, no. 4, pp. 619–630, Aug. 2014.

[5] S. Q. Zhou, W. Xu, K. Z. Wang, C. H. Pan, M.-S. Alouini, and A. Nallanathan, "Ergodic rate analysis of cooperative ambient backscatter communication," *IEEE Wireless Commun. Lett.*, vol. 8, no. 6, pp. 1679–1682, Dec. 2019.

[6] J. Kimionis, A. Bletsas, and J. N. Sahalos, "Increased range bistatic scatter radio," *IEEE Trans. Commun.*, vol. 62, no. 3, pp. 1091–1104, Mar. 2014.

[7] D. Bharadiay, K. Joshiy, M. Kotaru, and S. Katti, "BackFi: High throughput WiFi backscatter," *ACM SIGCOMM Comput. Commun. Rev.*, vol. 45, no. 4, pp. 283–296, Aug. 2015.

[8] S. H. Kim and D. I. Kim, "Hybrid backscatter communication for wireless-powered heterogeneous networks," *IEEE Trans. Wireless Commun.*, vol. 16, no. 10, pp. 6557–6570, Oct. 2017.

[9] S. Daskalakis, S. D. Assimonis, E. Kampianakis, and A. Bletsas, "Soil moisture scatter radio networking with low power," *IEEE Trans. Microw. Theory Tech.*, vol. 64, no. 7, pp. 2338–2346, Jul. 2016.

[10] G. Vougioukas, S. N. Daskalakis, and A. Bletsas, "Could battery-less scatter radio tags achieve 270-meter range?," in *Proc. IEEE Wireless Power Transfer Conf.*, Aveiro, Portugal, 2016, pp. 1–3.

[11] W. B. Wang, D. T. Hoang, D. Niyato, P. Wang, and D. I. Kim, "Stackelberg game for distributed time scheduling in RF-powered backscatter cognitive radio networks," *IEEE Trans. Wireless Commun.*, vol. 17, no. 8, pp. 5606–5622, Aug. 2018.

[12] X. Lu, D. Niyato, H. Jiang, E. Hossain, and P. Wang, "Ambient backscatter-assisted wireless-powered relaying," *IEEE Trans. Green Commun. Netw.*, vol. 3, no. 4, pp. 1087–1105, Dec. 2019.

[13] B. Lyu and D. T. Hoang, "Optimal time scheduling in relay assisted batteryless IoT networks," *IEEE Wireless Commun. Lett.*, vol. 9, no. 5, pp. 706–710, May 2020.

[14] B. Lyu, D. T. Hoang, and Z. Z. Yang, "Backscatter then forward: A relaying scheme for batteryless IoT networks," *IEEE Wireless Commun. Lett.*, vol. 9, no. 4, pp. 562–566, Apr. 2020.

[15] G. Yang, X. Y. Xu, and Y.-C. Liang, "Resource allocation in NOMA-enhanced backscatter communication networks for wireless powered IoT," *IEEE Wireless Commun. Lett.*, vol. 9, no. 1, pp. 117–120, Jan. 2020.

[16] Y. H. Ye, L. Q. Shi, R. Q. Y. Hu, and G. Y. Lu, "Energy-efficient resource allocation for wirelessly powered backscatter communications," *IEEE Commun. Lett.*, vol. 23, no. 8, pp. 1418–1422, Aug. 2019.

[17] S. H. Kim, S. Y. Park, K. W. Choi, T.-J. Lee, and D. I. Kim, "Backscatter-aided cooperative transmission in wireless-powered heterogeneous networks," *IEEE Trans. Wireless Commun.*, vol. 19, no. 11, pp. 7309–7323, Nov. 2020.

[18] Y. Wu, Y. F. He, L. P. Qian, J. W. Huang, and X. M. Shen, "Optimal resource allocations for mobile data offloading via dual-connectivity," *IEEE Trans. Mobile Comput.*, vol. 17, no. 10, pp. 2349–2365, Oct. 2018.

[19] X. Zhang, J. Tang, H.-H. Chen, S. Ci, and M. Guizani, "Cross-layer based modeling for quality of service guarantees in mobile wireless networks," *IEEE Commun. Mag.*, vol. 44, no. 1, pp. 100–106, Jan. 2006.

[20] J. Tang and X. Zhang, "Quality-of-service driven power and rate adaptation over wireless links," *IEEE Trans. Wireless Commun.*, vol. 6, no. 8, pp. 3058–3068, Aug. 2007.

[21] H. Su and X. Zhang, "Cross-layer based opportunistic MAC protocols for QoS provisionings over cognitive radio wireless networks," *IEEE J. Sel. Areas Commun.*, vol. 26, no. 1, pp. 118–129, Jan. 2008.

[22] X. Zhang and J. Tang, "Power-delay tradeoff over wireless networks," *IEEE Trans. Commun.*, vol. 61, no. 9, pp. 3673–3684, Sep. 2013.

[23] J. Tang and X. Zhang, "Cross-layer resource allocation over wireless relay networks for quality of service provisioning," *IEEE J. Sel. Areas Commun.*, vol. 25, no. 4, pp. 645–657, Apr. 2007.

[24] J. Tang and X. Zhang, "Quality-of-service driven power and rate adaptation for multichannel communications over wireless links," *IEEE Trans. Wireless Commun.*, vol. 6, no. 12, pp. 4349–4360, Dec. 2007.

[25] J. Tang and X. Zhang, "Cross-layer modeling for quality of service guarantees over wireless links," *IEEE Trans. Wireless Commun.*, vol. 6, no. 12, pp. 4504–4512, Dec. 2007.

[26] D. Mishra and E. G. Larsson, "Sum throughput maximization in multi-tag backscattering to multiantenna reader," *IEEE Trans. Commun.*, vol. 67, no. 8, pp. 5689–5705, Aug. 2019.

[27] Y. H. Al-Badarneh, M.-S. Alouini, and C. N. Georghiades, "Performance analysis of monostatic multi-tag backscatter systems with general order tag selection," *IEEE Wireless Commun. Lett.*, vol. 9, no. 8, pp. 1201–1205, Aug. 2020.

[28] D. Li, W. Peng, and F. Hu, "Capacity of backscatter communication systems with tag selection," *IEEE Trans. Veh. Technol.*, vol. 68, no. 10, pp. 10311–10314, Oct. 2019.

[29] J. Hajipour, A. Mohamed, and V. C. M. Leung, "Channel-, queue-, and delay-aware resource allocation in buffer-aided relay-enhanced OFDMA networks," *IEEE Trans. Veh. Technol.*, vol. 65, no. 4, pp. 2397–2412, Apr. 2016.

[30] N. Lee, F. Baccelli, and R. W. Heath Jr., "Spectral efficiency scaling laws in dense random wireless networks with multiple receive antennas," *IEEE Trans. Inf. Theory*, vol. 62, no. 3, pp. 1344–1359, Apr. 2016.

[31] E. Boshkovska, D. W. K. Ng, N. Zlatanov, A. Koelpin, and R. Schober, "Robust resource allocation for MIMO wireless powered communication networks based on a non-linear EH model," *IEEE Trans. Commun.*, vol. 65, no. 5, pp. 1984–1999, May 2017.

[32] E. Boshkovska, D. W. K. Ng, N. Zlatanov, and R. Schober, "Practical non-linear energy harvesting model and resource allocation for SWIPT systems," *IEEE Commun. Lett.*, vol. 19, no. 12, pp. 2082–2085, Dec. 2015.

[33] S. Z. Bi and Y. J. Zhang, "Computation rate maximization for wireless powered mobile-edge computing with binary computation offloading," *IEEE Trans. Wireless Commun.*, vol. 17, no. 6, pp. 4177–4190, Jun. 2018.

Authorized licensed use limited to: Texas A M University. Downloaded on January 17,2022 at 20:42:04 UTC from IEEE Xplore. Restrictions apply.

[34] Y. Wang, X. F. Tao, X. F. Zhang, P. Zhang, and Y. T. Hou, "Cooperative task offloading in three-tier mobile computing networks: An ADMM framework," *IEEE Trans. Veh. Technol.*, vol. 68, no. 3, pp. 2763–2776, Mar. 2019.

[35] M. Razaviyayn, M. Hong, and Z.-Q. Luo, "A unified convergence analysis of block successive minimization methods for nonsmooth optimization," *SIAM J. Optim.*, vol. 23, no. 2, pp. 1126–1153, Sep. 2012.

[36] S. Boyd, N. Parikh, E. Chu, B. Peleato, and J. Eckstein, "Distributed optimization and statistical learning via the alternating direction method of multipliers," *Found. Trends Mach. Learn.*, vol. 3, no. 1, pp. 1–122, Jul. 2011.

[37] Y. Yu, X. Y. Bu, K. Yang, H. Y. Yang, X. Z. Gao, and Z. Han, "UAV-aided low latency multi-access edge computing," *IEEE Trans. Veh. Technol.*, vol. 70, no. 5, pp. 4955–4967, Apr. 2021.

[38] C. M. Wang, C. C. Liao, F. R. Yu, Q. B. Chen, and L. Tang, "Computation offloading and resource allocation in wireless cellular networks with mobile edge computing," *IEEE Trans. Wireless Commun.*, vol. 6, no. 8, pp. 4924–4938, Aug. 2017.

[39] S. Boyd and L. Vandenberghe, *Convex Optimization*. Cambridge, U.K.: Cambridge Univ. Press, 2004.

[40] L. Q. Shi, Y. H. Ye, X. Y.Chu, and G. Lu, "Computation bits maximization in a backscatter assisted wirelessly powered MEC network," *IEEE Commun. Lett.*, vol. 25, no. 2, pp. 528–532, Feb. 2021.

[41] H. Y. Ding, D. B. D. Costa, X. D. Wang, U. S. Dias, R. T. de Sousa, and J. H. Ge, "On the effects of LOS path and opportunistic scheduling in energy harvesting relay systems," *IEEE Trans. Wireless Commun.*, vol. 15, no. 12, pp. 8506–8524, Dec. 2016.

[42] F. Wang, S. T. Guo, B. Xiao, Y. Yang, and X. Zhang, "Resource allocation and admission control for an energy harvesting cooperative OFDMA network," *IEEE Trans. Veh. Technol.*, vol. 67, no. 5, pp. 4071–4086, May 2018.

Fei Wang received the B.S. degree in mathematics from Liaocheng University, Liaocheng, China, in 2005, the M.S. degree from Wuhan University, Wuhan, China, in 2007, and the Ph.D. degree in computer science from Chongqing University, Chongqing, China, in 2012. She is currently an Associate Professor with Southwest University, Chongqing, China. She was a visiting Ph.D. student under the supervision of Professor Xi Zhang in the Networking and Information Systems Laboratory, Department of Electrical and Computer Engineering, Texas A&M University, College Station, TX, USA, from March 2017 to March 2018. Her research interests include resource allocation in wireless networks, network congestion control, and distributed algorithm design in wireless networks.

Xi Zhang (Fellow, IEEE) received the B.S. and M.S. degrees from Xidian University, Xi'an, China, the M.S. degree from Lehigh University, Bethlehem, PA, USA, all in electrical engineering and computer science, and the Ph.D. degree in electrical engineering and computer science (electrical engineering-systems) from the University of Michigan, Ann Arbor, MI, USA.

He is currently a Full Professor and the Founding Director of the Networking and Information Systems Laboratory, Department of Electrical and Computer Engineering, Texas A&M University, College Station, TX, USA. He is an IEEE Fellow for contributions to quality of service (QoS) theory in mobile wireless networks. He was with the Networks and Distributed Systems Research Department, AT&T Bell Laboratories, Murray Hill, NJ, USA, and AT&T Laboratories Research, Florham Park, NJ, USA, in 1997. He was a Research Fellow with the School of Electrical Engineering, University of Technology, Sydney, Australia, and the Department of Electrical and Computer Engineering, James Cook University, Australia. He has published more than 400 research papers on wireless networks and communications systems, network protocol design and modeling, statistical communications, random signal processing, information theory, and control theory and systems. He recieved the U.S. National Science Foundation CAREER Award in 2004 for his research in the areas of mobile wireless and multicast networking and systems. He received 6 best paper awards at IEEE GLOBECOM 2020, IEEE ICC 2018, IEEE GLOBECOM 2014, IEEE GLOBECOM 2009, IEEE GLOBECOM 2007, and IEEE WCNC 2010, respectively. One of his IEEE JOURNAL ON SELECTED AREAS IN COMMUNICATIONS papers has been listed as the IEEE Best Readings Paper (receiving the highest citation rate among all IEEE TRANSACTIONS/JOURNAL articles in the area) on wireless cognitive radio networks and statistical QoS provisioning over mobile wireless networking. He is an IEEE Distinguished Lecturer of the IEEE Communications Society and the IEEE Vehicular Technology Society. He received the TEES Select Young Faculty Award for Excellence in Research Performance from the College of Engineering at Texas A&M University, College Station, in 2006, and the Outstanding Faculty Award from Texas A&M University, in 2020.

Prof. Zhang is serving or has served as an Editor for IEEE TRANSACTIONS ON COMMUNICATIONS, IEEE TRANSACTIONS ON WIRELESS COMMUNICATIONS, IEEE TRANSACTIONS ON VEHICULAR TECHNOLOGY, IEEE TRANSACTIONS ON GREEN COMMUNICATIONS AND NETWORKING, and IEEE TRANSACTIONS ON NETWORK SCIENCE AND ENGINEERING. He served twice as a Guest Editor of IEEE JOURNAL ON SELECTED AREAS IN COMMUNICATIONS for Special Issue on "Broadband Wireless Communications for High Speed Vehicles" and Special Issue on "Wireless Video Transmissions." He was an Associate Editor for IEEE COMMUNICATIONS LETTERS. He served twice as the Lead Guest Editor for *IEEE Communications Magazine* for Special Issue on "Advances in Cooperative Wireless Networking" and Special Issue on "Underwater Wireless Communications and Networks: Theory and Applications." He served as a Guest Editor for *IEEE Wireless Communications Magazine* for Special Issue on "Next Generation CDMA vs. OFDMA for 4G Wireless Applications." He served as an Editor for Wiley's *Journal on Wireless Communications and Mobile Computing, Journal of Computer Systems, Networks, and Communications, and* Wiley's *Journal on Security and Communication Networks*. He served as an Area Editor for the Elsevier's *Journal on Computer Communications*, and among many others. He is serving or has served as TPC Chair for IEEE GLOBECOM 2011, the TPC Vice-Chair for IEEE INFOCOM 2010, the TPC Area Chair for IEEE INFOCOM 2012, the Panel/Demo/Poster Chair for ACM MobiCom 2011, the General Chair for IEEE WCNC 2013, and the TPC Chair for IEEE INFOCOM 2017-2019 Workshops on "Integrating Edge Computing, Caching, and Offloading in Next Generation Networks."

Authorized licensed use limited to: Texas A M University. Downloaded on January 17,2022 at 20:42:04 UTC from IEEE Xplore. Restrictions apply.